Deformation of Space-based Reflector Antennas

By
Frank J. Bonet
B.S., University of Kansas, 2018

Submitted to the graduate degree program in the Department of Aerospace Engineering and the Graduate Faculty of the University of Kansas in partial fulfillment of the requirements for the degree of Master of Science.

_____
Chair: Dr. Emily Arnold

_____
Dr. Richard Hale

_____
Dr. Mark Ewing

Date Defended: December 16th 2020

The thesis committee for Frank J. Bonet certifies that this is the approved version of the following thesis:

Deformation of Space-based Reflector Antennas

_____

Chair: Dr. Emily Arnold

Date Approved: December 16th 2020

Abstract

Space-based reflector antennas are susceptible to a variety of conditions that can result in surface deviation that affect the antenna's performance. This is especially true for small-satellite antennas, where the reflector surface is generally fabricated from flexible membrane materials that are folded for stowage during launch. In this work, various surface deviations are generated and simulated in an effort to characterize how differing surface deformations affect antenna performance metrics (i.e. maximum gain, relative side lobe levels, and beam width). The study utilizes a new surface generation tool to generate surfaces with both random and systematic errors. These surfaces are subsequently used in a commercial Finite Element Analysis (FEA) software to simulate the antennas. From the FEA results, antennas with larger reflector surfaces are shown to be less sensitive to surface errors, especially when the errors are random with low correlation length. Antenna performance is shown to be generally more sensitive to surface errors with larger correlation lengths. The surface Root Mean Square (RMS) is often used by a variety of analysis techniques to predict reflector antenna performance. One such method is Ruze's antenna tolerance theory. The FEA results are compared to Ruze's relatively simple analysis technique, and Ruze's method is shown to over predict gain losses, under predict side lobe level increases for surface errors with large correlation length, and is completely incapable of capturing any changes to half-power beam width. Finally, the FEA results illustrate that the metric of RMS alone is not sufficient to characterize expected changes in the radiation pattern. The results show that for the various surface error types and correlation lengths, the predicted values could be off by as much as 1 dB for gain loss, 1.5 dB for sidelobe levels, and 0.5^{o} for RMS values as small as $\lambda/70$.

Acknowledgements

I would like to thank my advisor, Dr. Arnold, for pushing me and providing me guidance through this process. As well, I would like to thank my parents for putting up with me throughout this during the pandemic. Finally, my friends in Lawrence deserves to be thanked for keeping my stress at a manageable level.

Table of Contents

List of Figures

List of Tables

1 Introduction

1.1 Background and Motivation

Parabolic reflector antennas are one of the most ubiquitous antenna types and are typically the antenna of choice for applications involving extraterrestrial signals (i.e. transmitting or receiving signals to/from space) due to their very high gains and directive beams. Examples of such applications include home satellite television, satellite communication links, and radio astronomy. The overall radiation characteristics and electrical performance of reflector antennas are critically related to the accuracy of the reflector surface. For antennas utilized on satellites where operational frequencies typically range from S- to Ka-band, surface errors on the order of 1 mm can results in a 2 dB gain loss [1]. Thus, there is significant interest in characterizing the effects of both random and systematic surface errors on the performance of reflectors.

Surface errors are caused by a variety of issues including manufacturing tolerances and loads caused by the many conditions and environments to which the antenna is subjected. Surface deviations in small-satellite reflector antenna applications are generally caused by stowage of the reflector during launch and the low stiffness of the membrane material. Warren et al. in [1] found that a CubeSat deployable membrane S-band reflector antenna exhibited a 2 dB loss in gain due to creases in the surface caused from folding the membrane during stowage. Similarly, Arya et al. in [2] observed a 0.5 dB gain loss when the surface root mean square of an X-band folding membrane reflector was only 0.5 mm. Chahat et al. developed a meshed surface Ka-band reflector which had a 0.5 dB gain loss from a 0.22 mm RMS surface distortion caused by folding [3].

While commercially available, physics-based finite element software is widely used to simulate and predict antenna performance, the effects of surface errors are typically assessed using analytical techniques such as Physical Optics (PO) and Geometric Optics (GO)/ray tracing, or by

experimentally characterizing the errors. Neither PO nor GO capture the full-wave response of the antenna like Finite Element Analysis (FEA) techniques can. These less robust analysis techniques and expensive experimental approaches are typically preferred over FEA, in part, due to the difficulties in generating the 3D CAD geometry of the deformed surface necessary for FEA analysis. In this work, a recently developed software tool called Antenna Deformation Tool (ADT) is used to generate continuous 3D reflector surfaces to enable full-wave simulations in commercial FEA software [4]. This work represents the first attempt to robustly characterize the performance effects of surface errors using FEA software.

The motivation for this work stems from the desire to more accurately predict antenna performance prior to the construction of the reflector surfaces. This is of particular importance for small form factor and deployable antennas necessary in small satellites applications. Clearly there is a tradeoff between antenna performance and system cost, weight, and volume when considering surface accuracy. Too loose of a tolerance may result in degradation beyond performance requirements, while too tight of a tolerance could lead to over development and excessive costs. As the demand for higher gain antennas with smaller form factors increases, there is an increasing need for more accurate and evolving simulation techniques.

The goal of this work is to examine the effects of both random and systematic surface errors on reflector antenna performance using FEA analysis and compare those results to the fast and efficient antenna tolerance theory developed by Ruze [5]. As will be discussed in Section 2.3, current analysis methods do not consider some or all the following effects: reflector edge diffraction, changes in the reflected signal angle, and the effects of the feed (i.e. blockage, scattering, and the feed's backward pattern contribution). By using commercial FEA software HFSS [6], all such effects can be considered. The FEA results will also be used to characterize the

sensitivity of the radiation pattern (i.e. gain, beam width, and side-lobe level) to various types and levels of surface errors. The FEA results for random surface errors will be compared against Ruze's antenna tolerance theory [5] which is a widely known work in the area and offers a rather simplistic solution to the problem.

Section 1.2 begins with a discussion of the work done to advance the previously discussed analysis techniques such as PO and GO. An overview of the characteristics/properties of parabolic reflector antennas and how these properties are affected by surface deformations is presented in Section 2. Section 3 presents the methodology used in this work to examine the sensitivity to the surface errors including design variables, model construction, and implementation of the surface errors when generating the modeling geometry. Finally, this paper concludes with the presentation and discussion of results from the FEA models in Sections 4 and a comparison to the commonly utilized Ruze method in Section 5. The major conclusions of the work as well as recommendations for future work is presented in Section 6.

1.2 Past Work

Common methods utilized in analyzing the radiation characteristics of reflectors are the aperture distribution method and the current distribution method which rely on PO and GO computational techniques. In the aperture distribution method, the field reflected by the surface of the paraboloid is first found over a plane normal to the axis of the reflector using GO techniques. This normal plane is typically coincident with the focal point and is called the aperture plane. Images depicting the focal point and the aperture plane are shown in Figure 1.1 and Figure 1.2, respectively. Next, equivalent sources are formed over the aperture plane (and assumed to be zero

outside the projected footprint of the reflector) and are subsequently used to compute the radiated fields.

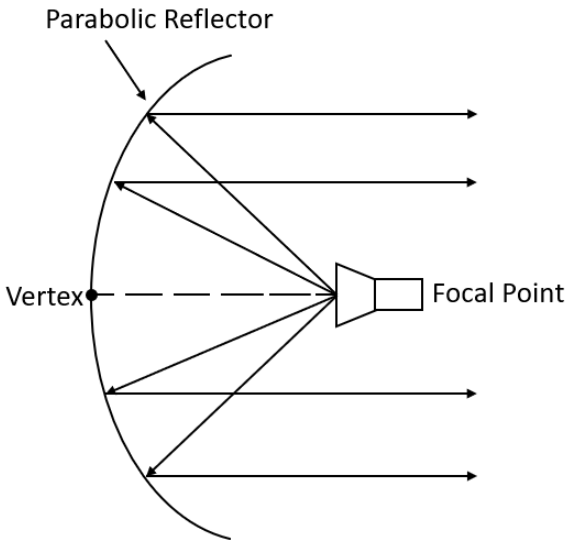

Figure 1.1: Focal Point of a Parabolic Reflector Antenna

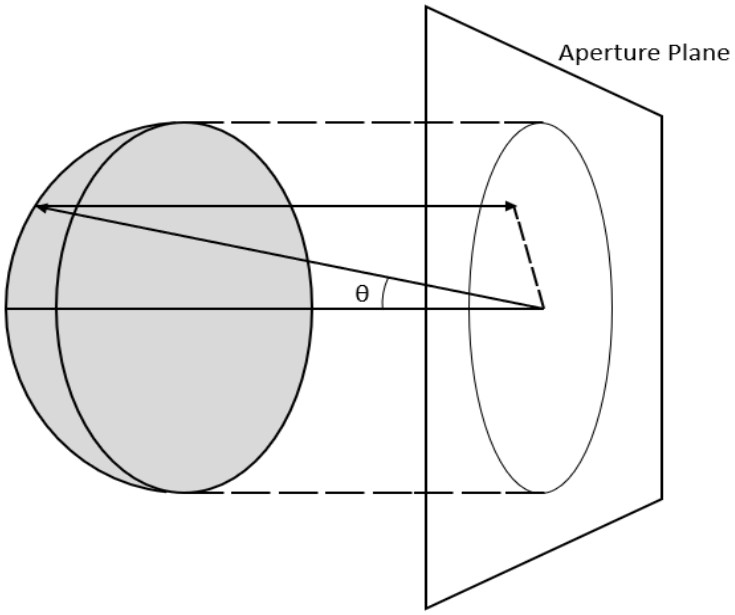

Figure 1.2: Aperture Plane of a Parabolic Reflector Antenna

The current distribution method approximates the induced current density over the illuminated side of the reflector using PO. From there, the current density is integrated over the

surface of the reflector to find the far-field radiation pattern. Both of these approaches assume that the current density is zero on the backside of the reflector surface, the discontinuity of the current density at the rim is neglected, and any effects of the feed (i.e. direct radiation or blockage) are also neglected. While these approaches provide good approximations for the main beam and small angle sidelobes, they are limited in their prediction capabilities without considering more sophisticated analyses such as geometrical diffraction techniques [7]. Furthermore, the accuracy of these techniques is further degraded in the presence of surface errors as the analysis techniques tend to only consider the phase errors resulting in path length errors.

An alternative approach to calculating the full radiation pattern from induced currents and reflected signals is to simply approximate the pattern based on the reflector geometry and the surface RMS error. The most well-known work in the area of reflector antenna surface errors comes from Ruze's antenna tolerance theory [5] which was first developed in the mid-1950's. This work is commonly utilized to predict changes in radiation patterns as a result of the random surface errors and utilizes a statistical approach to analyze the effects of random phase errors in the aperture. In the antenna tolerance theory, Ruze derived the relationships for determining the axial gain loss and pattern degradation based on the reflector surface RMS errors only. This theory assumes a Gaussian shape and distribution of errors while only considering path length errors when determining phase variations. From the Ruze method, it can also be shown that there exists a wavelength at which the gain reaches a maximum based on the surface RMS. While antenna tolerance theory has its limitations, this approach provides a simple and straightforward means to predict gain performance, and it can be adapted to any reflector antenna.

Zarghamee attempted to modify Ruze's work by modifying the assumption of the error distribution being uniform. This was developed in an attempt to improve Ruze's methodology,

resulting in a more accurate approximation of the illumination function. This distribution was modified to assume the surface RMS error is tapered as it approaches the edge of the reflector [9]. This change is minor unless the surface RMS is assumed to be much greater with respect to the operational wavelength of the reflector.

In an attempt to further improve this simplified approach, Cheng utilized a deterministic approach to analyze the pattern [10]. His methodology sought to better characterize the effects on the reflector parameters (i.e. gain, beamwidth, and sidelobe level) by considering the maximum phase error given for a specific antenna even without the exact phase direction. Through this approach, Cheng was able to determine the maximum gain loss from the maximum phase error on the aperture of the antenna. Furthermore, Cheng showed the largest reduction in half power beam width (HPBW) can be predicted from the maximum phase error.

Rahmat-Samii sought to develop a mathematical model to find the average pattern power loss from random surface errors [11]. In this method, the reflector surface is divided into ringed sections with the RMS value defined for each section. From these sections, individual radiation patterns are found before the average pattern is constructed. This method allows for non-uniform surface errors and illumination functions. Results from this model showed that antennas with relatively low sidelobe level (SLL) are most sensitive to the reflector surface errors [12].

Ghobrial and Jervase focused on changes to the cross-polarization of the signal due to surface errors [13]. The results of their paper show how the average cross-polarization from surface errors is affected by the surface RMS error, correlation diameter of the surface errors, and polarization efficiency. Furthermore, his work goes on to classify how the cross-polarization power of the main axis is affected by the magnitude of the surface RMS. Ghobrial found that for

small errors, the cross-polarization gain is directly proportional to the RMS, and for large errors ($\lambda > 0.04$), the cross-polarization is proportional to $\sqrt{1 - e^{-2rms^2}}$ [14].

Finally, Tripp determined pattern errors by utilizing a matrix scattering function which is calculated, assumed, or measured [15]. This approach is derived from the average power pattern in terms of the unperturbed aperture field with the scattering matrix. Additionally, a probability density function of the surface deformation positions is applied. With this method, the errors may be non-uniform and large, although this method is not commonly utilized due to complexity in the implementation of the surface error discretization.

While the aforementioned approaches provide quick solutions for determining reflector antenna performance in the presence of surfaces errors, these methods are limited in determining the affects to all antenna performance parameters (i.e. max gain, beamwidth, sidelobe levels, and cross polarization), as many of the studies focused solely on maximum gain or a specific performance parameter. This is in part due to the complex formulations necessary to derive each pattern characteristic. The method presented in this work seeks to classify the full spectrum of parameters for a generic reflector antenna by using robust FEA methods. The results generated using the FEA approach will also be compared to results generated from Ruze's original antenna tolerance theory. These two approaches represent opposite sides of the analysis spectrum as Ruze's method provides a quick and efficient solution at lower accuracy, while the FEA approach is more time intensive, but considers all physical phenomena contributing to the overall pattern. The FEA results will be used to help quantify the errors in Ruze's approximation.

2 Parabolic Reflector Antenna Characteristics

2.1 Reflector Geometry

A reflector antenna consists of the reflecting surface or surfaces and a radiating feed system. The purpose of a reflector is to focus the energy radiated from the feed, resulting in a narrow main beam with high gain. For most reflectors, the shape is defined by a revolved conic section such as a parabola, hyperbola, or ellipse. For many reflector antennas that operated from small satellites, the frequencies of operation range from S-band to Ka-band [16]. Most reflector antennas are classified into two major designs—front-fed and Cassegrain. Front-fed designs are a more basic design where the feed is placed at the focal point of the reflector, while Cassegrain designs have the feed mounted on the surface of the main reflector and a smaller reflector is placed at the focus [8]. To reduce complexity and overall computing time, this work focuses on front-fed designs.

Parabolic reflectors are among the most utilized reflector designs. The parabolic reflector surface is formed by rotating a parabola about its axis. From the parabolic shape of the reflector, the rays emanated from the focus point of the reflector are reflected in a manner that the rays become parallel (or collimated) to each other [8]. This is illustrated in Figure 2.1. Parabolic reflector surfaces can be mathematically defined using Equation 2.1 with spherical coordinates (i.e. r, θ, and ϕ). Due to rotational symmetry, the surface does not vary with respect to the surgical angle, ϕ [8].

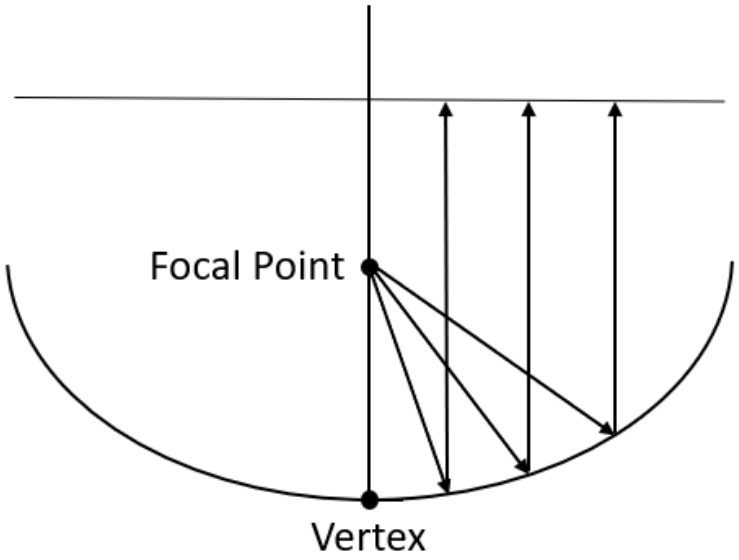

Figure 2.1: Two-dimensional configuration of a paraboloidal Reflector

$$r = \frac{2f}{1+\cos\theta} = f\sec^2\frac{\theta}{2} \quad \theta \leq \theta_0 \qquad \text{Equation 2.1}$$

Parabolic reflectors are often defined by the parameters of diameter, *D*, and focal length, *f*. More common, a parabolic reflector is often defined by the focal-to-diameter ratio f/D. These parameters represent the curvature of the dish when utilizing a fixed diameter *D*. For comparison of deployable reflectors, Table I shows the dimensions of various designs. Note the diameter size is defined in terms of multiples of the operating wavelength.

Table 2.1: Small Satellite Antennas and their design properties

	Operating Frequency, (GHz)	**Diameter, (λ)**	**f/D**
Ka PDA [3]	35.7	59.6	0.5
ISARA [18]	26.0	37.0	0.67
MarCO HGA [19]	8.4	19.2	-
DaHGR [16]	10.0	20.0	0.5
OMERA [17]	36.0	166.9	-
KaTENna [2]	36.0	120.1	-

In Equation 2.1, θ_0 represents the angle from the main axis to the outer portion of the reflector, called the subtended angle. The relation between the subtended angle and the f/D ratio is shown in Equation 2.2 and 2.3 [8].

$$\theta_0 = 2\,\mathrm{atan}\left(\frac{1}{4f/D}\right) \qquad \text{Equation 2.2}$$

$$f/D = \frac{1}{4\tan(\theta_0/2)} \qquad \text{Equation 2.3}$$

These equations of a parabolic reflector show how the curvature of the reflector is defined by the ratio f/D.

2.2 Parabolic Reflector Antenna Properties

A parabolic reflector exhibits high gain because the reflect rays are collimated and in-phase due to the identical path lengths from the feed point to the aperture plane. The aperture plane is a surface that is perpendicular to the direction of maximum radiation depicted in Figure 1.2.

A major component of the reflector antenna system is the feed which affects the reflector antenna's amplitude, phase, and field polarization. It is important for the feed to radiate in a way that it appears to radiate from a single point. This condition can be achieved by the feed having a spherical phase front and a relatively small size. Furthermore, the feed should radiate most of the energy into the reflector surface to avoid energy spill over while also having a uniform amplitude over a wide angle to cover the full area of the reflector. After energy from the feed is reflected, all waves are polarized in the same direction. However, feed radiation can be wasted by the perpendicular polarized component of the aperture field contribution to side lobes [20]. The

depiction of principal and cross-polarization components in a parabolic reflector antenna is illustrated in Figure 2.2 [21].

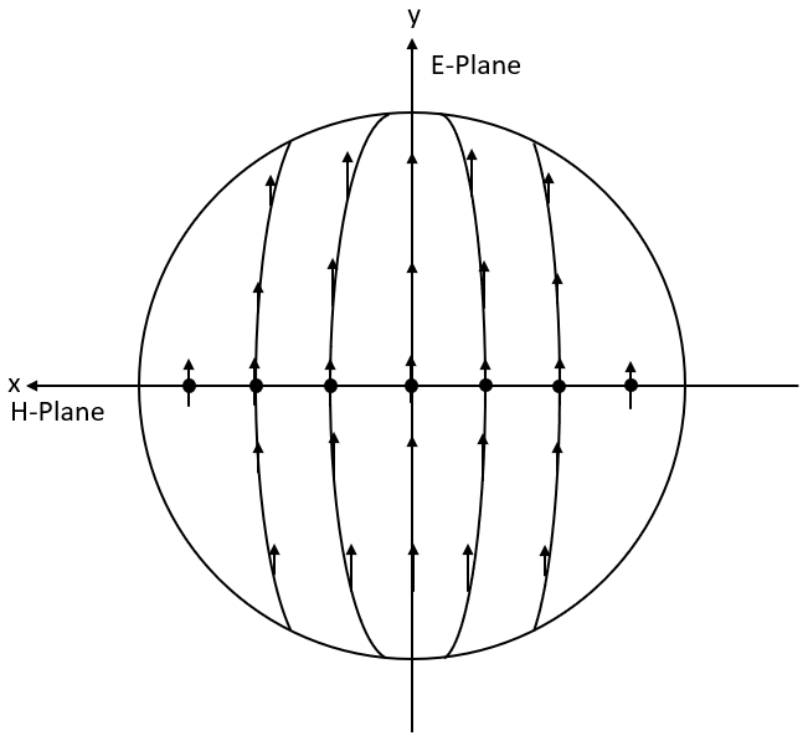

Figure 2.2: Principal and Cross-polarization components of a Paraboloidal Reflector

Parabolic reflectors are highly effective at a wide range of frequency bands with the tailoring of the design easing at lower frequency ranges. Reflectors designed to perform at higher frequency bands are limited by the smoothness of the reflector surface [22]. Distortion of the surface must be much less than a fraction of a wavelength to avoid significant phase errors in the aperture. Often a maximum value surface error (RMS) of $\lambda/20$ is used as a reference [8]. These deformations could lead to losses in antenna performance such as gain, directionality, and overall performance.

2.2.1 Reflector Antenna Radiation Pattern

The radiation pattern or antenna pattern is defined as a mathematical function or a graphical representation of the radiation properties of the antenna as a function of spherical coordinates [8]. Most often, this radiation pattern is determined in the far-field region and is represented as a function of the angular variation. A representation of a typical radiation pattern for a parabolic reflector antenna is shown in Figure 2.3. The peak at 0^o is called the main lobe. This region contains the highest intensity of radiation in the pattern due to the fields from the reflector being the most in-phase along this direction. Peaks in the pattern outside the main lobe are classified as side lobes, and generally it is desirable to minimize the power in these lobes. Furthermore, the cross-polarization component of the antenna pattern in shown in the figure with the blue line. For a parabolic reflector, the antenna is primarily linearly polarized as shown in Figure 2.2, and the cross-polarization pattern is typically very low in power and has a null in the direction of the main lobe.

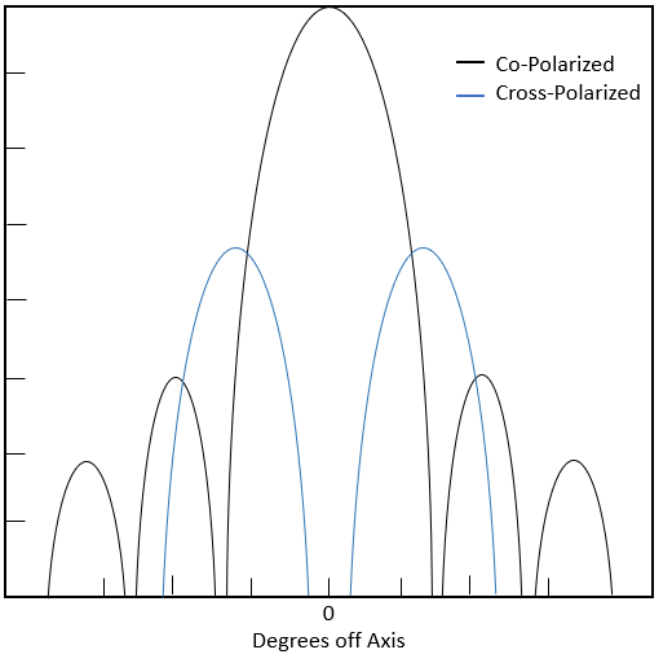

Figure 2.3: Parabolic Reflector Radiation Pattern

As previously stated, the radiation pattern is defined as a mathematical function in a spherical coordinate system. From geometry and feed variables, techniques can be used to calculate the antenna radiation pattern. Geometric optics is a common approach utilized in finding the radiation pattern. This high-frequency analysis process utilizes raytracing to determine the current distribution on an aperture plane. The current distribution is then utilized to derive the radiation pattern of the reflect antenna [23]. As computing power increases, other analysis techniques for determining radiation patterns are introduced. Finite element analysis (FEA) can be utilized for analyzing specific antenna setups to high precision. Such simulations for parabolic reflector antennas can be simple to set up and analyzed in a relatively short amount of time. Details on FEA analysis techniques relevant to this work will be presented in Section 3.

2.3 Effects of Surface Errors on the Performance of Reflectors

Reflector surfaces subjected to environmental effects and those that utilize deployment mechanisms are subject to a variety of surface errors. These surface deformations degrade the amplitude and phase of the fields on the aperture resulting in a reduction of gain, increase in side lobe levels, and increase in HPBW [24]. This section will discuss how each reflector property is affected by the surface accuracy.

Small satellite reflector antennas have a unique set of technical issues as compared to terrestrial antennas. In these applications, surface distortions are caused by thermally induced strain, manufacturing tolerances, structural design, and folding of mesh reflectors to accommodate stowage during launch. Surface errors experienced by these (and other) reflectors can be classified into two major categories--random errors and systematic errors. Random errors typically arise

from manufacturing tolerances or creasing/wrinkling in flexible membrane surfaces required for stowage. Random surface errors are typically smaller in amplitude as compared to systematic errors. Systematic errors in the surface arise from gravitational and thermal factors and are dependent on the design of the support structure. In some cases, systematic errors can be compensated for by utilizing adaptive reflector surfaces and electromagnetic compensation techniques [25]. The following sections describe the general effects of these surface errors on antenna performance properties.

2.3.1 Gain

Gain, $G(\theta, \phi)$, represents the intensity of the radiation as a function of the spherical coordinates shown in Figure 2.4.

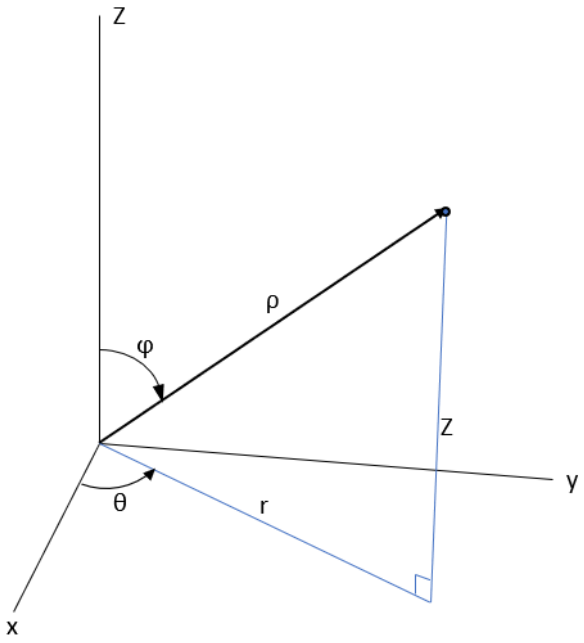

Figure 2.4: Representation of Spherical Coordinates

The gain of an antenna can be measured experimentally and is defined as the directivity, $D(\theta,\phi)$, times antenna efficiency,e_{cd} , in the direction of θ and ϕ. The directivity is the ratio of the radiation intensity, $U(\theta,\phi)$ to total power radiated, P_{rad}. These relations are shown in Equations 2.4 and 2.5 [8].

$$D(\theta,\phi) = 4\pi \frac{U(\theta,\phi)}{P_{rad}} \qquad \text{Equation 2.4}$$

$$G(\theta,\phi) = e_{cd} D(\theta,\phi) \qquad \text{Equation 2.5}$$

The maximum gain of a parabolic reflector antenna is given by Equation 2.6. Where D is the diameter of the aperture, λ is the wavelength, and η_{ap} is the efficiency of the aperture [8].

$$G_{max} = \eta_{ap} \left(\frac{\pi D}{\lambda}\right)^2 \qquad \text{Equation 2.6}$$

Through the equation, it is obvious that as the wavelength decreases the maximum gain increases. In practice, the gain is limited by the deviations on the antenna surface from the optimal shape. From Ruze's antenna tolerance theory, the maximum gain is reduced by exponential factors relating to surface RMS, ϵ_{rms} , as shown in Equation 2.7 [8].

$$G(\theta,\phi) = G_0(\theta,\phi) e^{-\overline{(2\epsilon_{rms})^2}} + \left(\frac{(2\pi c)}{\lambda}\right)^2 e^{-\overline{(2\epsilon_{rms})^2}} \sum_{n=1}^{\infty} \frac{\left(\overline{(2\epsilon_{rms})^2}\right)^2}{n*n!} e^{-\frac{\left(\frac{\pi c u}{\lambda}\right)^2}{n}} \qquad \text{Equation 2.7}$$

From Equation 2.7 it is evident that the introduction of surface errors degrades the main lobe most significantly due to the spatial term u = sin(θ) [8]. The reduction in gain is directly related to the defocusing of the beam caused by the surface errors as well as the changes in the field polarization on the reflector surface (refer to Figure 2.2). Thus, the surface deformations not only decrease the power in the co-polarization pattern, but also increase the power in the cross-polarization pattern because opposing fields no longer cancel.

2.3.2 Side Lobe Levels

Side lobe levels (SLL) are reported relative to the maximum gain as a representation of how the power is distributed between the main beam and the side lobes. Reflectors are often designed with a tradeoff involving the efficiency of the aperture and side lobe levels [11]. With this tradeoff, the amplitude of the aperture field is tapered towards the edge of the reflectors to reduce the amplitude of the side lobes. These efforts may still cause slight degradation in the main beam and aperture efficiency due to the Fourier relationship between the aperture field and the far field.

Reflector surface errors lead to an increase in the side lobes in a radiation pattern. Reflector antennas with low side lobe level requirements tend to have a tighter requirement on the surface accuracy because it is shown that side lobes degrade much quicker when surface errors are introduced [5]. Thus, a side lobe requirement is often the design driver for a reflector antenna.

2.3.3 Half Power Beam Width

Half-power beam width is the reflector's ability to focus the main beam. This parameter measures the spread in the angle of the main beam between the points of half-power, hence the name half-power beam width. The beam width of the antenna is further classified by the beam efficiency, which is defined as the ratio of power radiated in the main beam region to the total

power radiated [7]. When surface errors are present, the main beam widens which reduces the overall antenna efficiency [25]. For satellite applications, this degradation in the beam width is particularly problematic due to the antenna's distance from the target. The large separation between the source and the target results in a large illuminated area. Thus, the effects from reflector surface errors are shown to decrease gain and relative sidelobe levels, as well increase the half power beam width of reflector antennas.

3 Methodology

This section discusses the methods utilized to generate the deformed reflector surfaces as well as the simulation setup for the various designs. The process begins with the construction of the non-uniform rational B-spline surfaces (NURBS) in MATLAB [26]. This discussion includes how the various reflector surface types are differentiated and how the deformations of the surfaces are applied. Then, the specifics of the finite element analysis within the bounds of the HFSS modeling software is discussed. Finally, the procedures utilized for the data processing used in the display of results in Section 4 will be presented.

3.1 Geometry Construction

3.1.1 Reflector Properties

The representative geometry used for the analysis was a circular parabolic reflector. An f/D ratio and diameter were selected to define the size and curvature of the surface. Given the diameters and f/D values presented in Table I, a value of 0.416 for f/D was selected while the diameter was determined by the wavelength of the antenna. A rectangular horn was used as the feed antenna, and it was designed to operate at 10 GHz, similar to that of other small satellite antennas, which resulted a wavelength of 30 mm. With the wavelength defined, two different sized reflectors were chosen for this study—20λ and 40λ—which covers a range representative of small satellite deployable reflect antennas [15].

3.1.2 Creation of Reflector Surfaces

The reflector surfaces are generated utilizing a custom MATLAB program called the Antenna Deformation Tool, or ADT [4]. ADT first generates a point cloud representative of the

parabolic reflector shape. After the nominal surface point cloud has been generated, either random or systematic errors are applied to the point cloud based on a prescribed RMS error. With the control points defined in the point cloud, ADT converts the points into a non-uniform rational B-spline (NURBS) surface.

Two types of deformed surfaces are created for the study, random and systematic error distributions. For the random surface error, ten surfaces were generated using the prescribed RMS values to try to capture the average performance of the random geometry. In addition, two different variants of the random surface were created by using a variable number of control points. The two variants have the same RMS; however, the "smooth" surface has more gradual changes in the surface, while "rough" surface variations have a much smaller period. Fewer control points were used to generate a surface with "smooth" variations, while more control points resulted in a "rough" surface. For this study, 1,000 control points represent the "smooth" deformed surfaces, and 10,000 control points represent the "rough" deformed surfaces. To characterize the "smooth" and "rough" surfaces, the autocorrelation of each is shown in Figure 3.1 and Figure 3.2, respectively. The correlation length is the distance over which the correlation coefficient falls to e^{-1}, and for each surface type (i.e. "smooth" and "rough") the calculated correlation lengths are 0.0636 and 0.0168 of the normalized radii respectively [27].

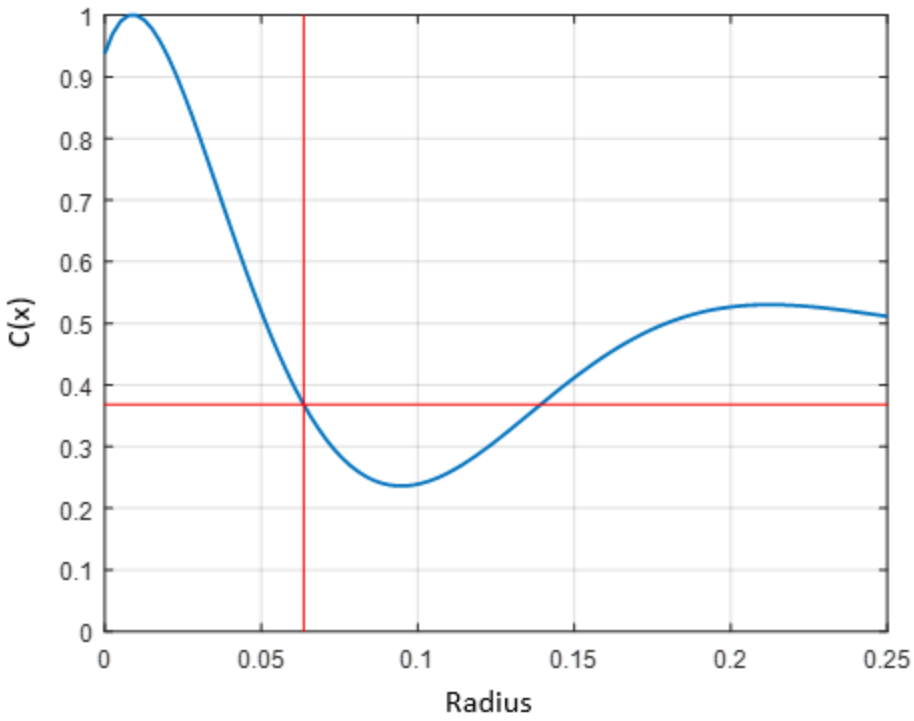

Figure 3.1: Correlation Function for Smooth Surface

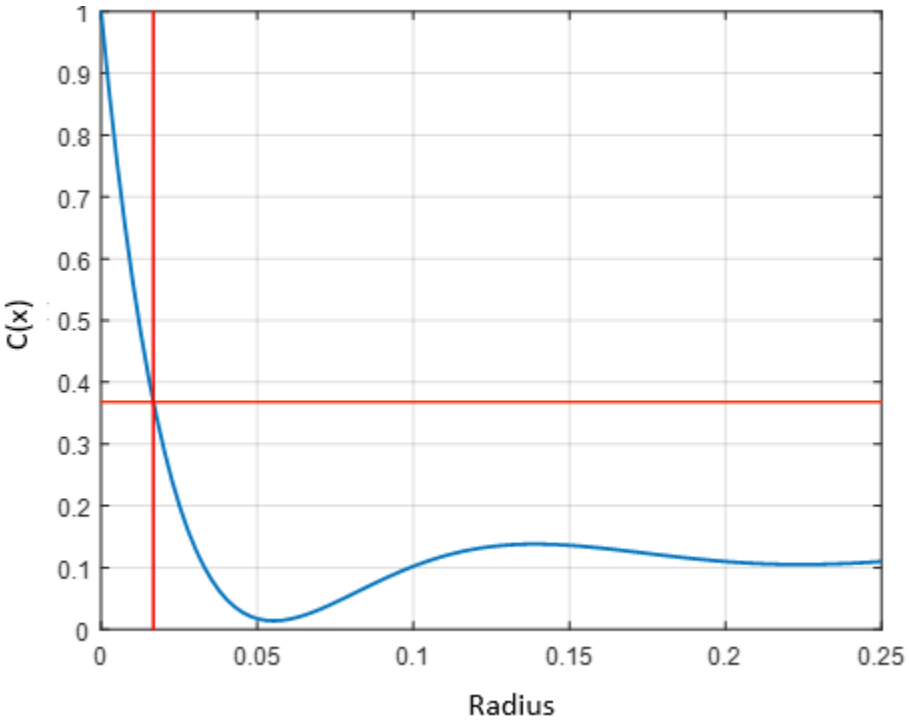

Figure 3.2: Correlation Function for Rough Surface

3.1.3 Application of Surface Errors

The randomly deformed surfaces are created by applying a z-translation to the control points of the "smooth" and "rough" surfaces resulting in the prescribed RMS surface error. The applied random errors use a normal distribution over all the control points with the RMS equivalent to one standard deviation. The prescribed surface RMS errors were chosen to be $\lambda/10$, $\lambda/15$, $\lambda/20$, $\lambda/30$, $\lambda/40$, $\lambda/50$, $\lambda/60$, and $\lambda/70$. These variations in surface deformations were chosen to represent deformities greater than and less than the standard criterion of $\lambda/20$ and to values seen in produced deployable designs [8]. For each of the random RMS configurations, ten variant surfaces were created to determine the average performance of a surface with comparable attributes. A heat map of the representative reflector surfaces with random errors at an RMS error of $\lambda/20$ is shown in Figure 3.3.

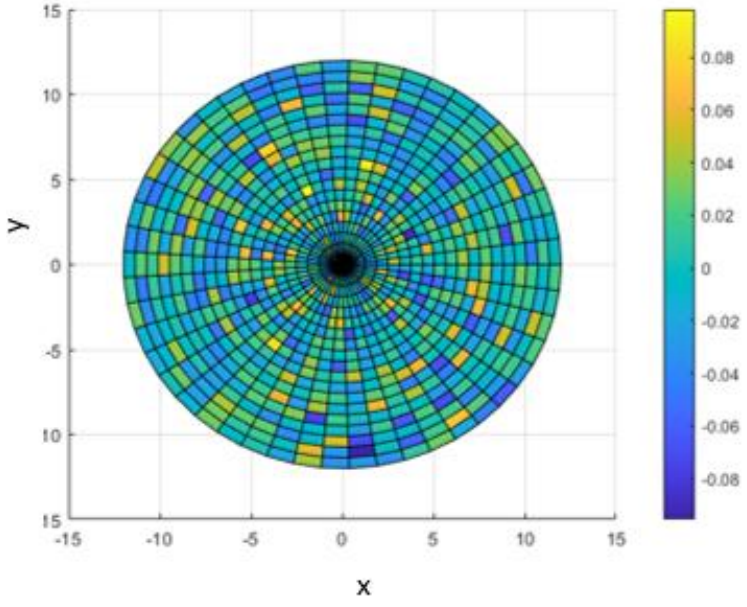

Figure 3.3: Heat Map for Random Error Application on Reflector Surface

The surfaces generated through this method are then compared to the undeformed reflector in the program Siemens NX [28]. This is done to ensure the validity of the created surfaces in MATLAB by verifying the RMS of the surfaces matches the RMS specified. Using the Deviation Gauge tool in NX, points on the surfaces of the undeformed reflector to the points on the surface of the deformed reflectors are compared. A depiction of the NX deviation gage tool is shown in Figure 3.4, visualizing the surface deviation in a $\lambda/20$ reflector with a maximum positive deformation of 0.294 inches and a maximum negative deformation of 0.271 inches. Utilizing the information and point differences provided through the tool in Siemens NX, the RMS is calculated by using 50 points. This surface comparison study was conducted on the five surfaces for each 20λ reflector variant. This is documented in Table A.1 showing each surface distribution and the maximum variation in surface RMS in Appendix A. From the table shown, each of the measured surface RMS values are shown to fall within a maximum deviate from the intended vale of ~2%. From these surface measurements, the resulting surfaces are shown to be representative of the intended RMS surface values.

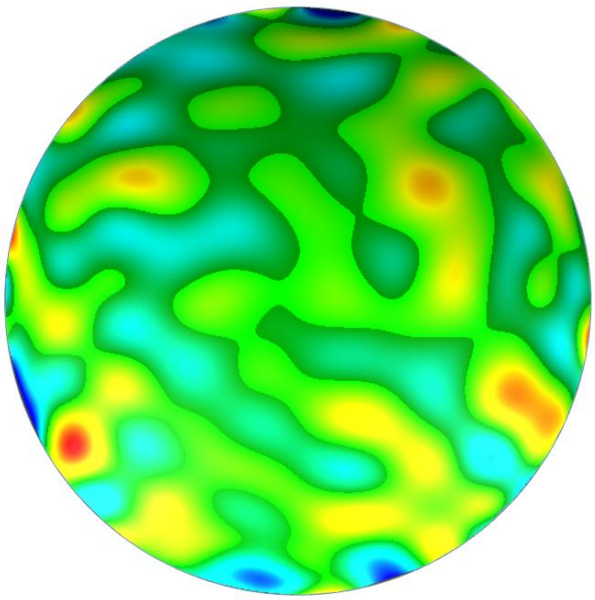

Figure 3.4: NX Deviation Gauge Tool of a λ/20 Reflector

Systematic deformations were also applied to the surfaces and are representative of deformations shown through common thermally induced strain conditions [29]. These deformations are also comparable to those due to deployment mechanisms and support structures. For systematic deformations, structures with four and six segments were chosen to represent reflectors with similar designs [16]. The surfaces were deformed with amplitudes which represent the RMS values chosen in the random deformation section. Equation 3.1 defines the systematic errors applied to the surfaces with n representing the number of node lines on the surface (n is utilized as 2 and 3). This equation from [30] represents the thermal deformations experienced in a circular reflector with varying hard point locations. A heat map of the representative reflector surfaces with systematic errors at an RMS error of $\lambda/20$ is shown in Figure 3.4

$$\Delta z(\rho, \phi) = d_0 \left(\frac{\rho}{D/2}\right)^n \cos(n\phi) \qquad \text{Equation 3.1}$$

In Equation 3.1, Δz represents the deformation at each point on the surface as a function of the polar coordinates ρ and ϕ, and d_0 is the maximum deformation of the surface at the maximum diameter, D. Given that the errors are deterministic, only a single reflector surface is required for each case.

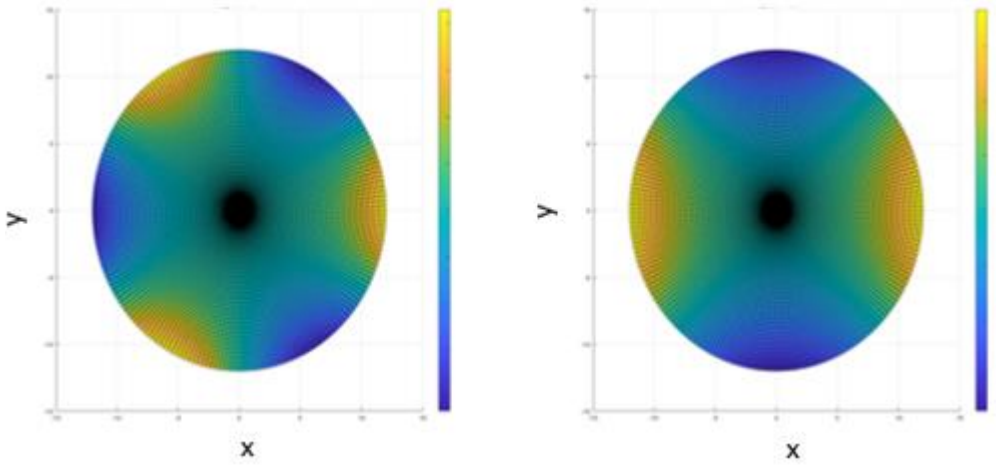

(a) (b)

Figure 3.5: Heat Map for Systematic Error Application on Reflector Surface; (a) Represents the Surface Utilizing n = 3 and (b) with n = 2

After the surfaces were generated using ADT, the resulting NURBS surfaces were converted to a Parasolid and imported into ANSYS HFSS 2019 R2 for simulation.

3.2 FEA Simulation Setup

Prior to conducting the simulations with the various reflector surfaces, the feed antenna had to be modeled. A horn antenna was constructed with regards to the specifications discussed in Section 3.1.1. For this horn antenna, a wave port is constructed in HFSS and placed at the surface in the narrow section of the horn. A drawing depicting the dimension variables of the representative horn is shown in Figure 3.4.

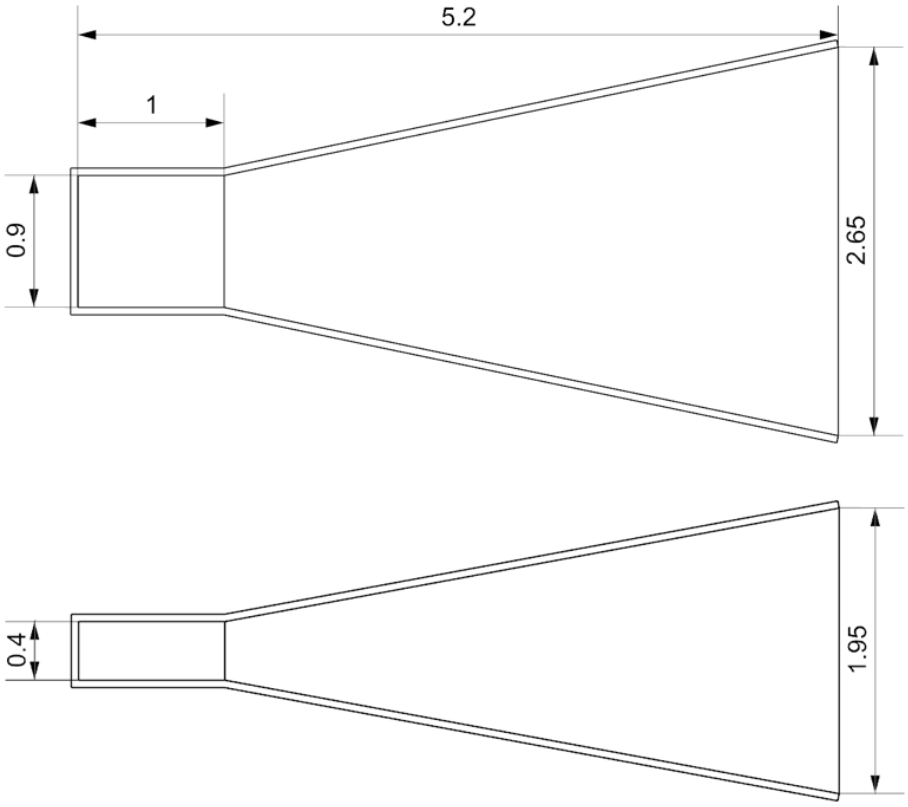

Figure 3.6: Representative Wave Guide Fed Horn Antenna, All Dimensions in inches (Not to Scale)

After the horn was modeled, the various reflector surfaces were added to the model. The horn was placed at the approximate location of the focal point of the reflector surface. The location is described as "approximate" given that the exact location of the horn phase center was unknown. For the 20λ and 40λ reflectors, the horn was placed 279.4 and 476.25 mm from the center of the reflector surfaces, respectively.

As mentioned earlier, the finite element analysis simulations for the reflectors are performed utilizing the commercial software package, HFSS Ver. 19. A parametric analysis was first conducted to determine the ideal placement of the horn since the location of the horn phase center is somewhat ambiguous. The location of the horn that resulted in the largest gain was determined

to be the focal point. The HFSS default library property for aluminum is utilized for the horn, and the reflector was given the properties of a perfect electric conductor (PEC). For the 20λ reflector a volume around each of the components was defined and prescribed as a vacuum bounded by a Finite Element Boundary Integral (FEBI) hybrid radiation boundary. The edges of the volumes of the applied air boxes were spaced λ/4 from the edges of the antenna surfaces, as is standard practice. Figure 3.5 depicts the simulation workspace for the constructed model [31]. The modeling approach used in these designed is called the finite element boundary integral approach, and it combines the generality and robustness of the Finite Element Method (FEM) with the efficiency of the Integral Equation (IE) approach by only requiring solution volumes around the surface and feed antenna (as opposed to one large volume around both). The solution approach starts by computing the fields on the air box bounding surfaces using an absorbing boundary condition. This information is then passed to HFSS's integral equation solver which computes a correction to the boundary fields. These corrections are then passed back to the FEM solver. This process is repeated until the solution converges.

When the simulation is scaled up to the large reflector, the model construction is slightly altered due to simulation time and computer RAM limitations. In this case, no vacuum volume is applied around the reflector surface and instead, a Hybrid IE region is applied to the reflector itself. The solution space in HFSS for these models is shown in Figure 3.6.

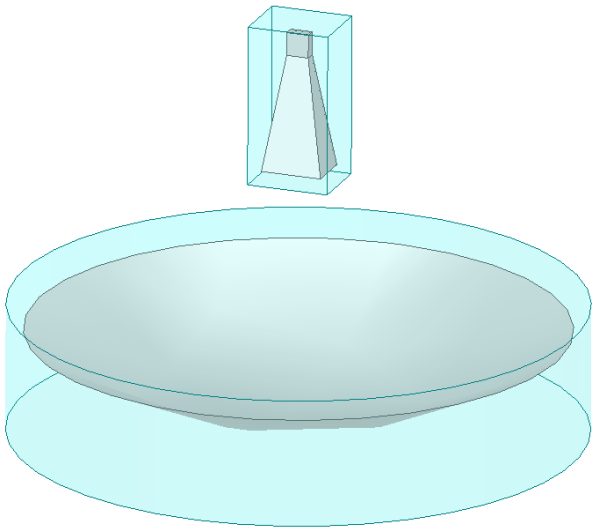

Figure 3.7: HFSS Model Created for the 20λ Reflector Antenna

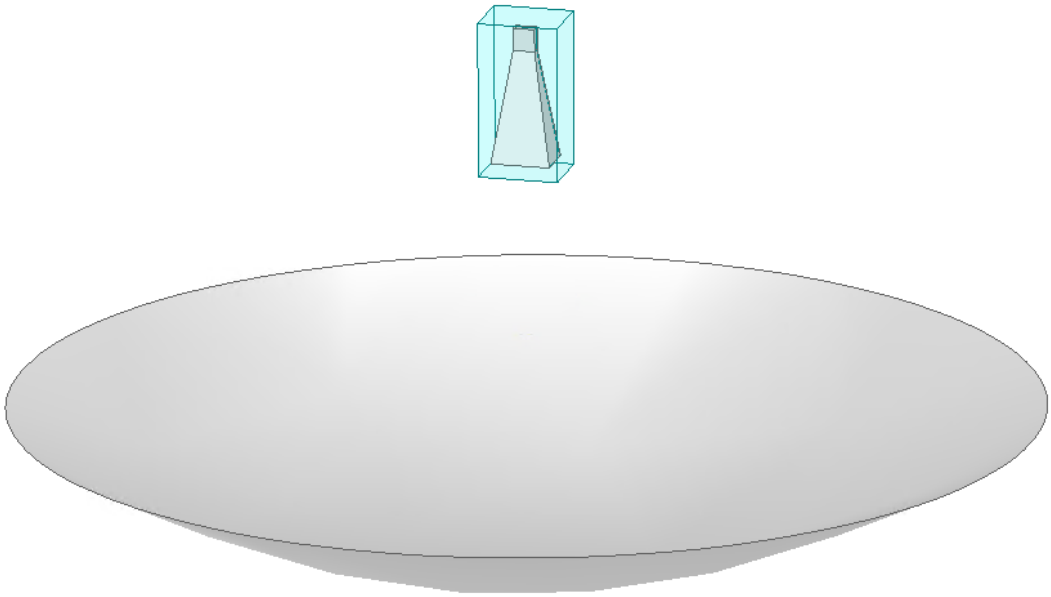

Figure 3.8: HFSS Model Created for the 40λ Reflector Antenna

This solution setup is prone to negligible errors as compared to the FEBI approach. Appendix B provides results for both the FEBI and IE methods for the 20λ reflector. The difference

in the two solutions was shown to be less than 0.15 dB change in maximum gain, 0.1 dB change in side lobe levels, and 0.1^{o} change in beam width. These small errors are attributed to the lack of modeling free space radiation without an airbox present [30].

A total of 160 models were created to capture all the variations in reflector size and surface errors. For these simulated models, a minimum and maximum number of iterations prescribed in the solution setup was 2 and 12 respectively, and each model was verified to converge under the S perimeter (scattering parameter of the single antenna frequency) convergence criteria before the maximum iterations where reached. With this convergence criteria, the solution was specified to converge when the maximum ΔS turn reached less than 0.02. This convergence would occur on average after 4 to 5 iterations in the 20λ reflector and 3 iterations in the 40λ reflector. Though the HFSS analysis, this convergence is achieved with each pass/iteration of the solver refining the FEA mesh. Thus, the simulations conducted in HFSS are shown to provide valid results. The following section summarizes the results of the simulations.

4 FEA Simulation Results

This section presents the results of the simulated models utilizing the process discussed in Section 3. First, the nominal values of the base reflectors will be presented. These results will serve as a baseline to which the deformed results will be compared. Performance metrics such as maximum gain, relative sidelobe levels, and HPBW will be assessed for both random and systematic errors. In Section 5 these results will be compared to the theoretical results derived from Ruze's classical antenna tolerance theory.

4.1 Establishing a Baseline

Figure 4.1 and Figure 4.2 depict the radiation pattern for the non-deformed (or nominal) representative reflectors with diameters 20λ and 40λ, respectively. Table 4.1 summarizes the nominal antenna values. As expected, the larger reflector produces higher gain, lower relative side lobe levels, and a much narrower main beam. In the following section, the deformed reflector results will be compared to the nominal results presented in Figure 4.1 and Figure 4.2.

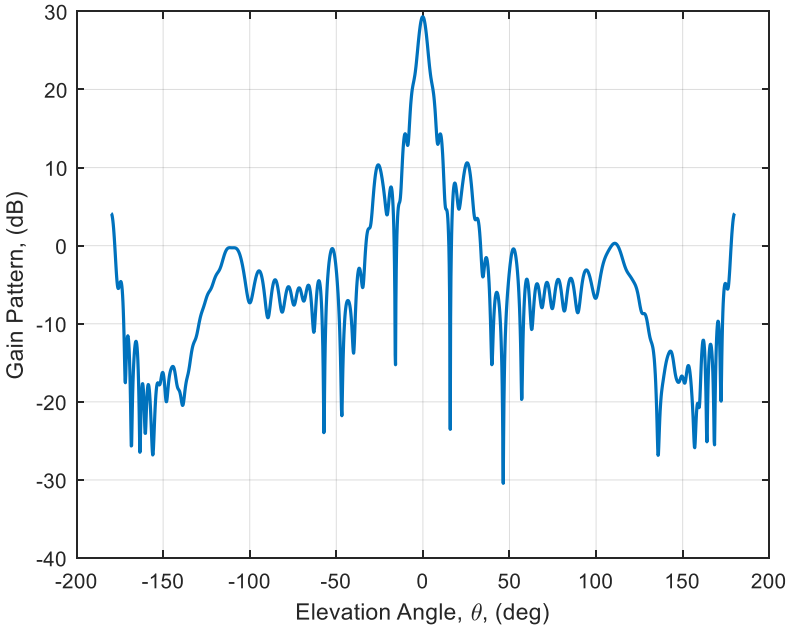

Figure 4.1: 20λ Nominal Radiation Pattern

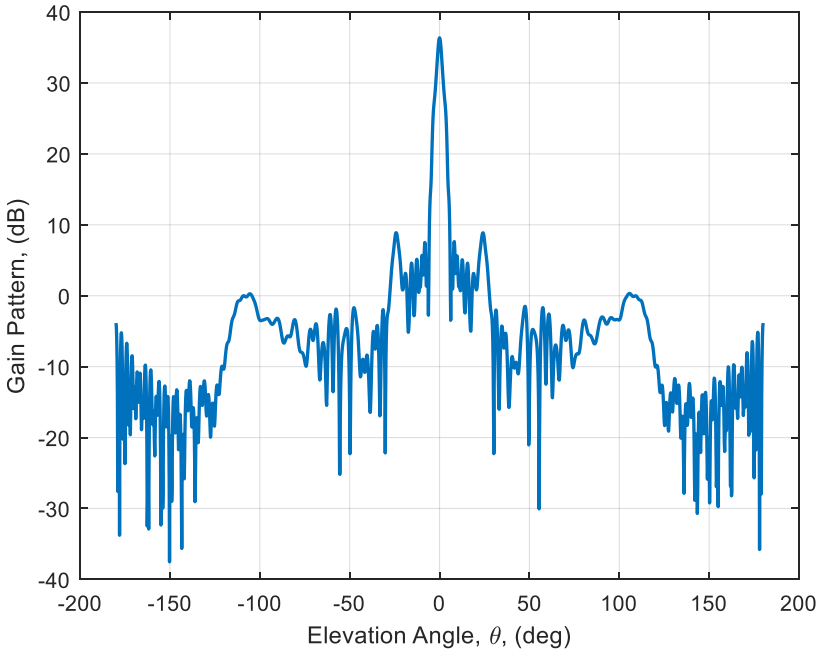

Figure 4.2: 40λ Nominal Radiation Pattern

Table 4.1: Nominal Reflector Values

Reflector Properties	20λ Diameter	40λ Diameter
Maximum Gain (dB)	29.3	36.4
Relative Side Lobe Level (dB)	-15.5	-27.5
HPBW (deg.)	4.9	2.5

4.2 FEA Surface Errors Application

4.2.1 20λ Reflector Random Surface Errors

As described in Section 3.1.3, a variety of surface distortions were applied to the reflector surface to examine performance degradation in presence of surface errors. This section will present the results for the smaller reflector with random surface errors with variable RMS roughness. RMS values were varied from $\lambda/70$ to $\lambda/10$ for two different correlation lengths representing "smooth" variations and "rough" variations. These random surface errors are representative of errors caused by manufacturing tolerances or wrinkles from stowage of a membrane reflector. Figure 4.3 through

Figure 4.5 show the radiation pattern comparison between the smooth and rough random deformations applied to the 20λ reflector. These figures presented the three largest deformation cases of $\lambda/10$, $\lambda/20$, and $\lambda/30$, respectively. Only the plots for these cases are presented as the changes in the patterns become more subtle at lower RMS values. However, these cases do capture RMS values on either side of the commonly used design standard of λ/20. [14]. The lower end of displayed deformations was chosen to be λ/30 because the radiation patterns with surface RMS less than λ/30 begin to converge to the nominal pattern and would be difficult to decipher changes in the pattern. The radiation pattern performance metrics (i.e. gain, SLL, and HPBW) for each distortion case is summarized in Table 4.2.

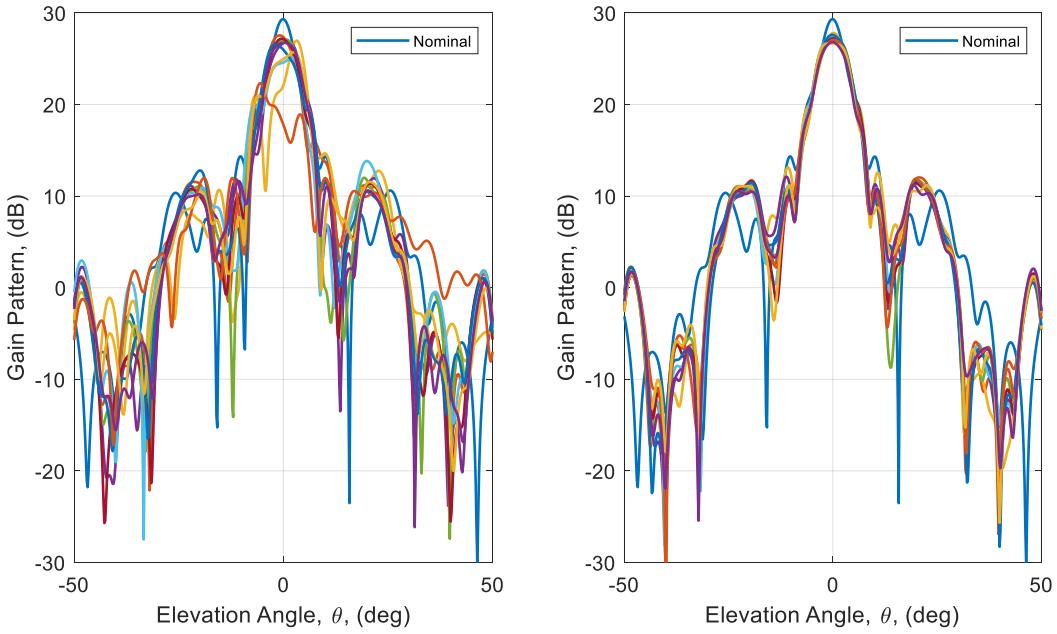

Figure 4.3: λ/10 Smooth (Left) and Rough (Right) Ten Random Error Radiation Patterns and Nominal Pattern for 20λ Reflector

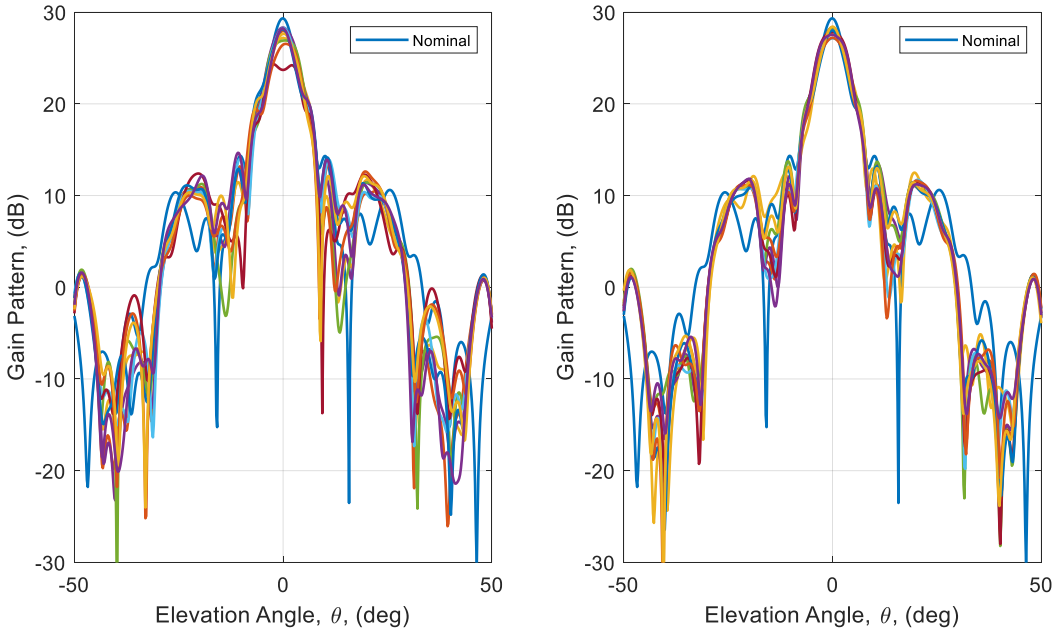

Figure 4.4: λ/20 Smooth (Left) and Rough (Right) Ten Random Error Radiation Patterns and Nominal Pattern for 20λ Reflector

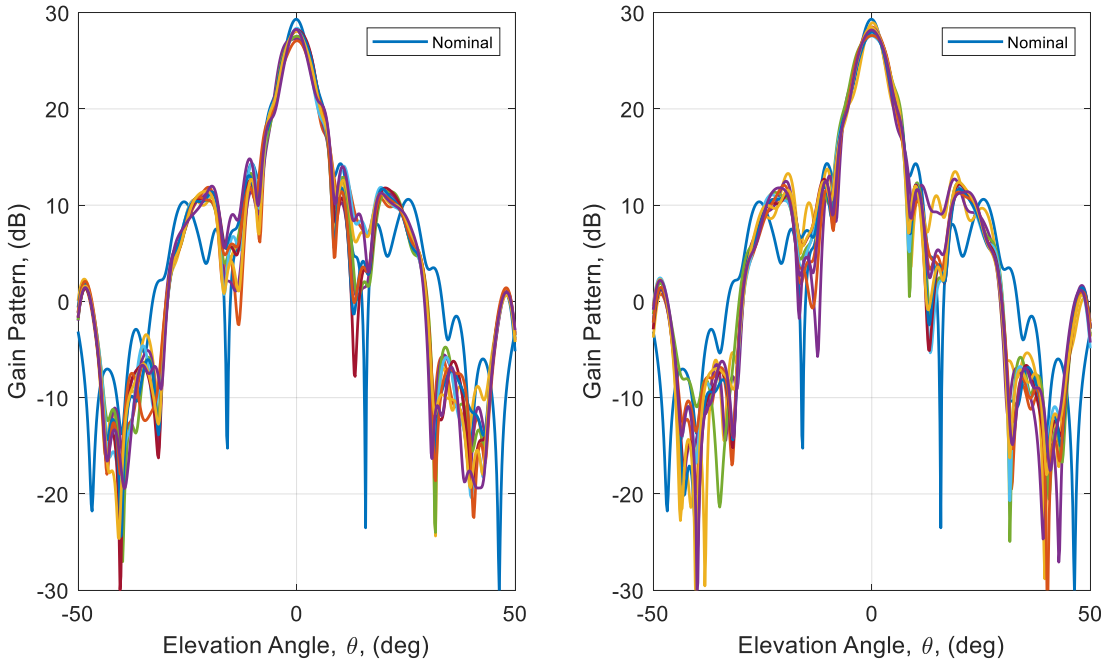

Figure 4.5: λ/30 Smooth (Left) and Rough (Right) Ten Random Error Radiation Patterns and Nominal Pattern for 20λ Reflector

For the smooth error results, at high surface errors (i.e. $\frac{\lambda}{20}$and greater), the main beam has the potential to split, which was not observed for the smaller distortion cases). This phenomenon is shown in Figure 4.3 and Figure 4.4. A simple qualitative assessment of the patterns in the figures, reveals that the smooth surface variations cause more severe pattern distortions than rough variations, especially with regards to the main beam shape, power, and SLL. Furthermore, this assessment of rough to smooth pattern variation shows the splitting of the main beam in reflectors with surface errors of λ/10 and λ/20. For a better qualitative assessment Table 4.2 has been provided to summarize the average performance metrics for all levels of surface RMS.

Table 4.2: Average Values for the 20λ Reflector Antenna Performance Properties for Surfaces Subjected to both Smooth and Rough Random Errors

	Max Gain (dB)		Relative SLL (dB)		HPBW (deg.)	
RMS	**Smooth**	**Rough**	**Smooth**	**Rough**	**Smooth**	**Rough**
λ/10	26.2	27.2	-10.2	-15.4	6.8	7.4
λ/15	27.1	27.7	-14.8	-15.2	7.0	7.2
λ/20	27.4	27.8	-14.4	-15.4	6.6	6.6
λ/30	27.9	28.1	-14.9	-15.6	6.5	6.6
λ/40	28.0	28.5	-14.1	-15.4	6.1	6.0
λ/50	28.1	28.5	-14.9	-15.1	6.0	5.7
λ/60	28.3	28.8	-14.7	-15.3	5.5	5.3
λ/70	28.3	28.5	-14.8	-15.1	5.6	5.7
Nominal	29.3	-	-15.5	-	4.9	-

From Table 4.2, it is apparent that the gain loss is higher for smooth surface errors than rough errors. For the highest surface error case, λ/10, the smooth error case had an additional 1 dB in gain loss as compared to the rough errors. The difference in gain loss reduces to 0.2 dB for the λ/70 case, but the smooth errors consistently result in lower gain. When compared to the nominal case, even the smallest surface errors result in about 1 dB in gain reduction.

The smooth surface error relative sidelobe levels are consistently 1 to 0.5 dB higher than that of the rough reflector surface; however, for the smallest surface error case, the SLL seems to converge to the nominal value. Interestingly, it seems the half power beam width appears to be more focused for the smooth errors higher surface RMS, while at lower surface RMS the smooth and rough surface errors converge to within 0.2^o of each other. In both instances, even the smallest errors result in an approximate 0.7^o increase in beam width for both cases.

In general, it is shown that the 20λ reflector is much more sensitive to smooth surface errors rather than rough surface errors. With the exception of the beam width at RMS values greater than λ/40, the smooth RMS case always resulted in lower antenna pattern performance. With the exception of the SLL, which seem to converge to the nominal value (and actually performs better for rough surface errors), the results indicate that surface errors as small as λ/70 result in a reduction in pattern performance on the order of 1 dB for gain and 0.7^o for beam width.

4.2.2 40λ Reflector Random Surface Errors

The radiation patterns for the larger 40λ reflector with smooth and rough random error deformations are presented in Figure 4.6 through Figure 4.8. Table 4.3 provides an overview of the average antenna performance values (max gain, relative side lobe levels, and half power beam width) from all simulated values of the 40λ surfaces. Similar to the 20λ reflector only surface errors of $\lambda/10$, $\lambda/20$, and $\lambda/30$ are provided.

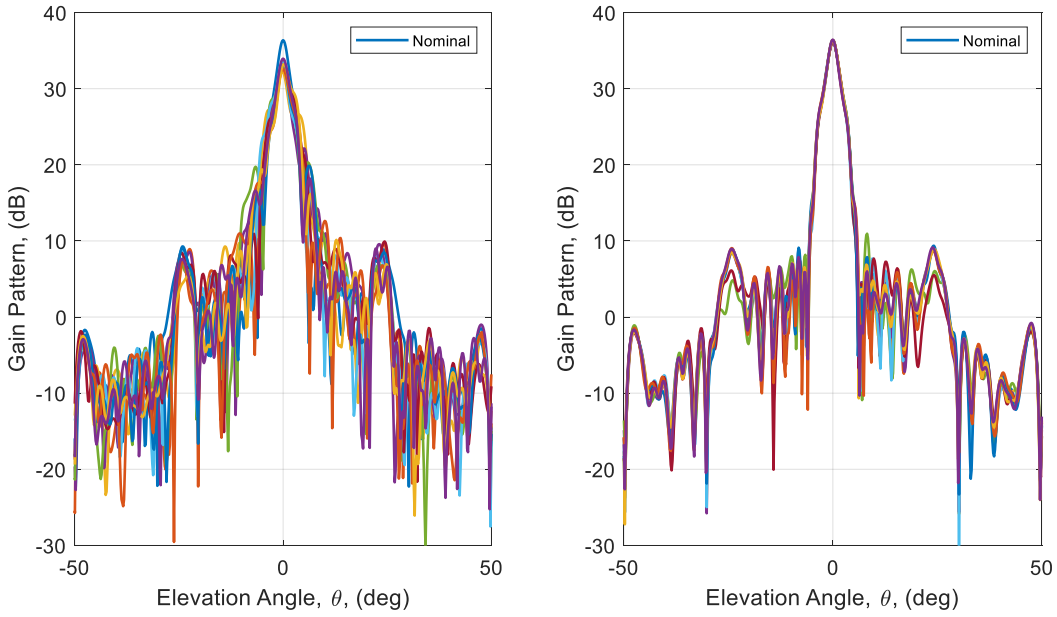

Figure 4.6: λ/10 Smooth (Left) and Rough (Right) Ten Random Error Radiation Patterns and Nominal Pattern for 40λ Reflector

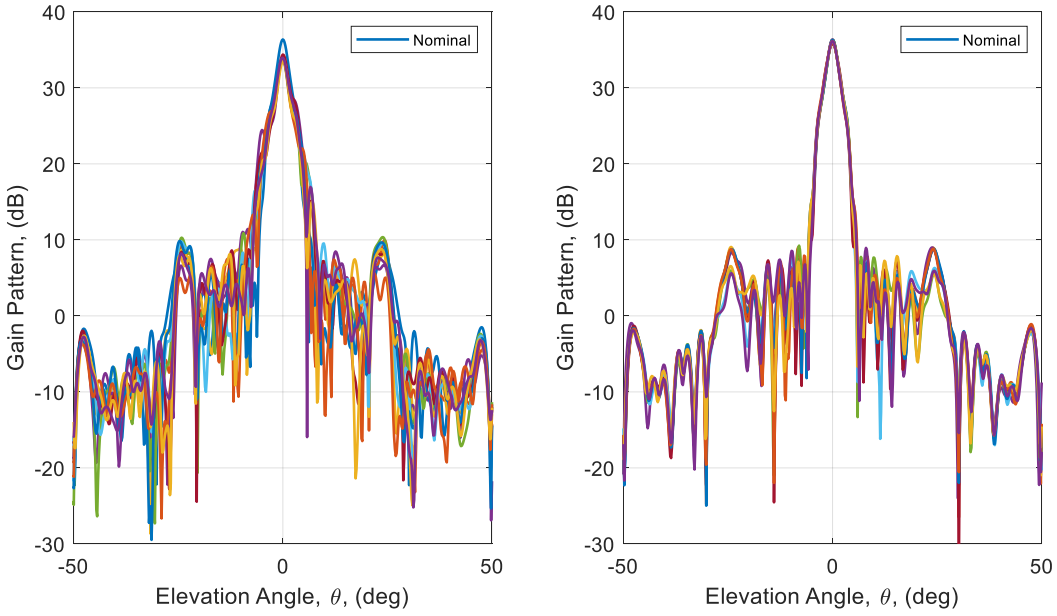

Figure 4.7: λ/20 Smooth (Left) and Rough (Right) Ten Random Error Radiation Patterns and Nominal Pattern for 40λ Reflector

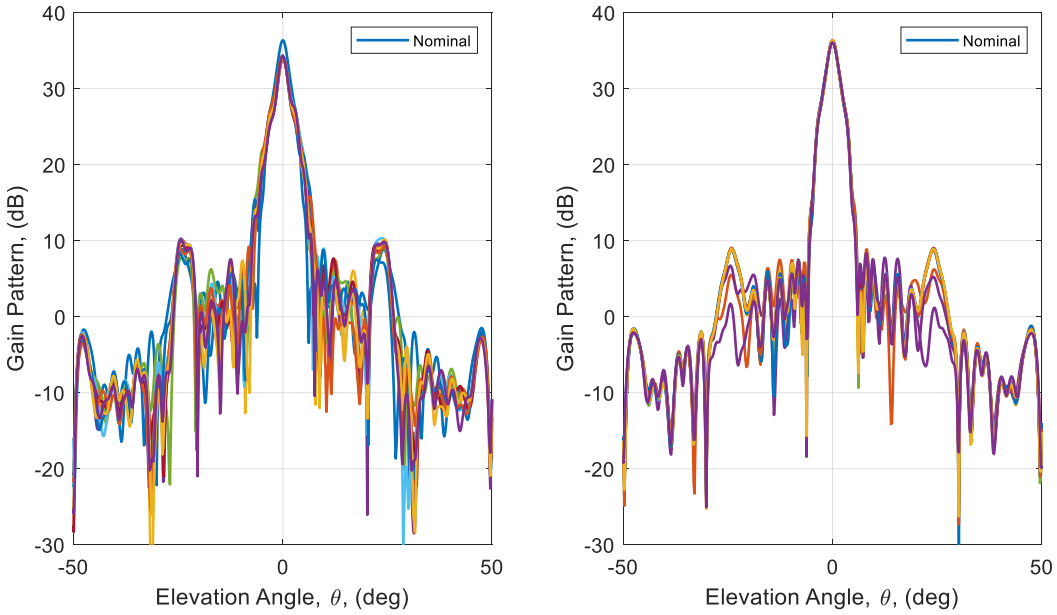

Figure 4.8: λ/30 Smooth (Left) and Rough (Right) Ten Random Error Radiation Patterns and Nominal Pattern for 40λ Reflector

Table 4.3: Average Values for the 40λ Reflector Antenna Performance Properties for Surfaces Subjected to both Smooth and Rough Random Errors

	Max Gain (dB)		Relative SLL (dB)		HPBW (deg.)	
RMS	**Smooth**	**Rough**	**Smooth**	**Rough**	**Smooth**	**Rough**
λ/10	33.2	36.3	-14.9	-27.3	2.7	2.5
λ/15	33.8	36.2	-18.7	-27	2.5	2.5
λ/20	33.9	36.2	-20.0	-27.3	2.4	2.6
λ/30	34.2	36.3	-20.1	-27.5	2.4	2.5
λ/40	36.2	36.2	-26.7	-27.5	2.6	2.5
λ/50	36.2	36.1	-27.7	-27.6	2.6	2.6
λ/60	36.2	36.2	-27.2	-27.2	2.5	2.6
λ/70	36.1	36.3	-27.3	-27.4	2.6	2.5
Nominal	36.4	-	-27.5	-	2.5	-

When comparing the radiation pattern plots of the larger reflector to the smaller reflector with smooth errors, the larger reflector appears to not have the same level of variance in the main beam and side lobes as the smaller reflector. This is especially apparent by the fact that the main beam is never split in any instance.

Interestingly, the gain for the rough RMS case seems to be insensitive to the surface distortions, regardless of the distortion level. This is true for all performance metrics in the case of rough RMS, and in general, the larger reflector appears to be insensitive to rough surface errors. Regardless of surface RMS, the gain, SLL, and HPBW of the larger reflector stayed within 0.3 dB, 0.5 dB, and 0.1^o, respectively. These pattern changes are smaller than those observed for the smallest of smooth RMS values for the smaller reflector.

Similar to the 20λ reflector, the smooth RMS case results in a 3.2 dB gain loss for the highest distortion case. However, unlike the 20λ reflector case, all performance metrics of the larger reflector tend to converge towards the nominal values. As mentioned previously, the gain, SLL, and HPBW were only off by 0.3 dB, 0.2 dB, and 0.1^o, respectively, for the smallest surface distortions. By comparing the results in Table 4.2 and Table 4.3, it is evident that for RMS values less than λ/40 the larger the reflector surface, the less sensitive the performance is to surface deviations. The only pattern metric where the larger reflector performed worse than the smaller reflector was the SLL for RMS values greater than λ/40. The SLL were ~13 dB higher in the λ/10 case for the larger reflector compared to only ~5 dB for the smaller reflector.

4.2.3 Systematic Surface Error

Using Equation 3.1 in Section 3.1.3, systematic errors representative of thermally induced strain and deployment mechanisms utilized on small satellites were generated [18][26]. Since the errors are deterministic, each case was only simulated once. The results of the systematic error for both the 20λ and 40λ reflectors with 3 node lines (i.e. n = 3 in Eq. 3.1) are shown in Figure 4.9 through Figure 4.11. As well, the results for the reflectors with 2 node lines (i.e. n = 2 in Eq. 3.1) are shown in Figures 4.12 through Figure 4.14. In addition, both the 0^o and 90^o azimuth patterns

are shown for RMS values ranging from λ/10 to λ/30. Though the deformations are symmetric, the two azimuth patterns differ slightly because of the oblong pattern of the feed horn. Table 4.4 summarizes the performance results for both reflectors with systematic errors.

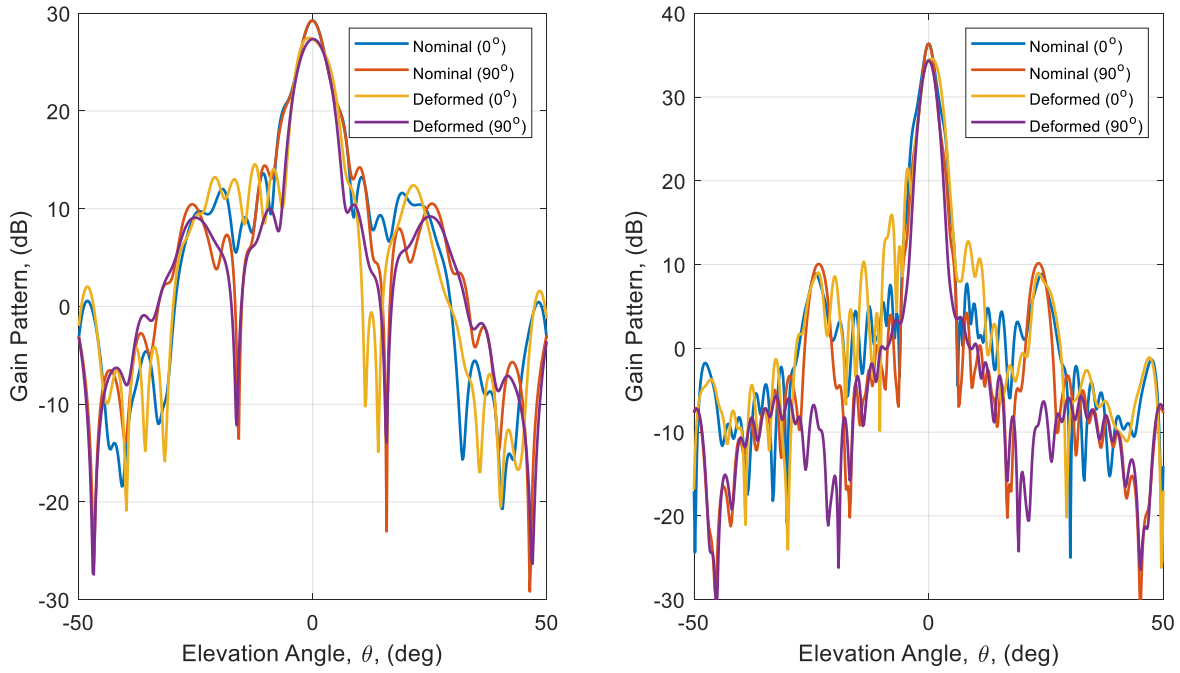

Figure 4.9: Systematic Radiation Patterns (n = 3) with RMS = λ/10 for 20λ (Left) and 40λ (Right) Reflectors

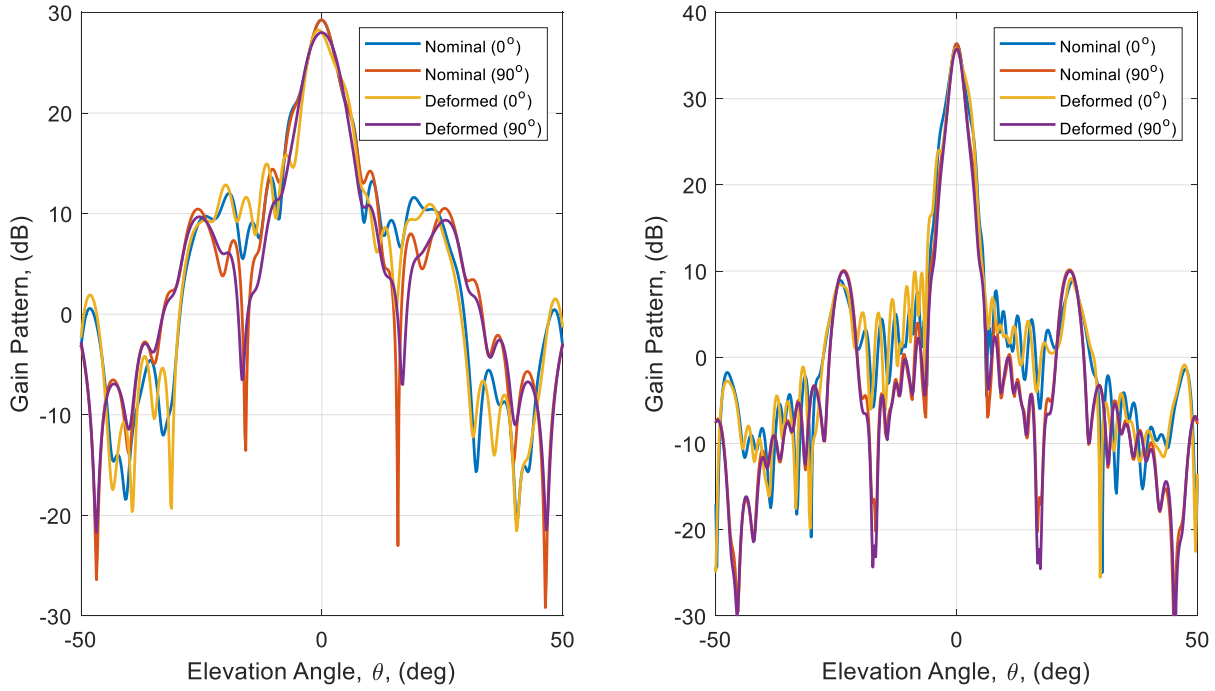

Figure 4.10: Systematic Radiation Patterns (n = 3) with RMS = λ/20 for 20λ (Left) and 40λ (Right) Reflectors

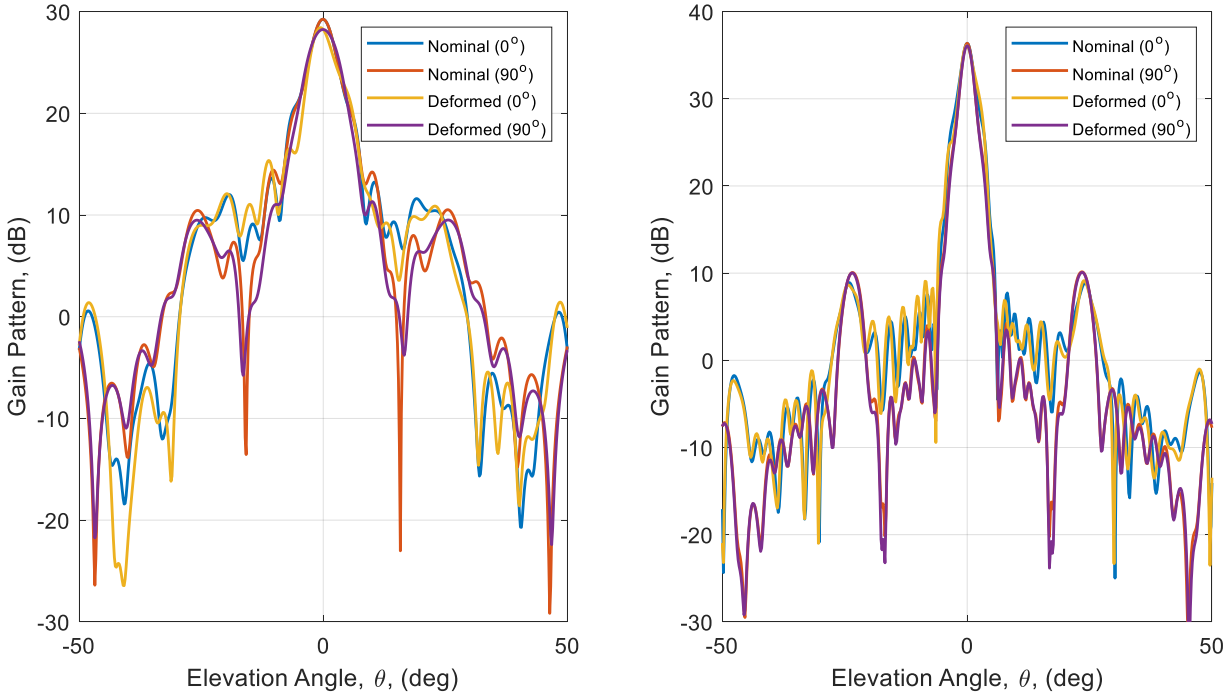

Figure 4.11: Systematic Radiation Patterns (n = 3) with RMS = λ/30 for 20λ (Left) and 40λ (Right) Reflectors

Table 4.4*:* Average Values for the Reflector Antenna Performance Properties for 20λ and 40λ Surfaces Subjected to Systematic Errors (n = 3)

	Max Gain (dB)		Relative SLL (dB)		HPBW (deg.)	
RMS	**20λ**	**40λ**	**20λ**	**40λ**	**20λ**	**40λ**
λ/10	27.5	34.6	-12.9	-13.1	7.2	3.8
λ/15	28.4	35.5	-12.2	-25.6	6.5	3.4
λ/20	28.3	35.8	-12.4	-25.9	6.4	2.9
λ/30	28.4	36.1	-11.9	-26.0	6.4	2.6
λ/40	28.5	36.2	-11.8	-26.1	6.3	2.6
λ/50	29.1	36.3	-15.0	-26.2	5.0	2.5
λ/60	29.3	36.3	-14.6	-26.2	5.1	2.5
λ/70	29.4	36.3	-14.7	-26.2	5.0	2.5
Nominal	29.3	36.4	-15.5	-27.5	4.9	2.5

The simulated results of the systematic errors applied to the larger 40λ reflector show similar trends to that of the random smooth surface error results presented in Section 4.2. More specifically, the rate at which the parameters of maximum gain, sidelobe levels, and half power beam width degrade as the RMS of the surface increases is similar to that of the 20λ reflector with smooth error distribution. Furthermore, the degradation in variables presented in Table 4.4 are similar for both the 20λ and 40λ reflectors. Both sized reflectors have a drop of about 2 dB in maximum gain improving to within 0.2 dB of their nominal values for surface RMS values of $\lambda/50$ and below. For the largest surface errors, both reflectors exhibit a SLL increase of ~2 dB. However, for the larger reflector, the relative SLLs show the trend settling at a 1 dB increase in SLL, whereas the smaller reflector converges to within 0.3 dB of the nominal value. The HPBW for the reflectors has an increase of about 1.5^{o} converging to within 0.1^{o} of the nominal values for surface RMS values of $\lambda/50$ and below.

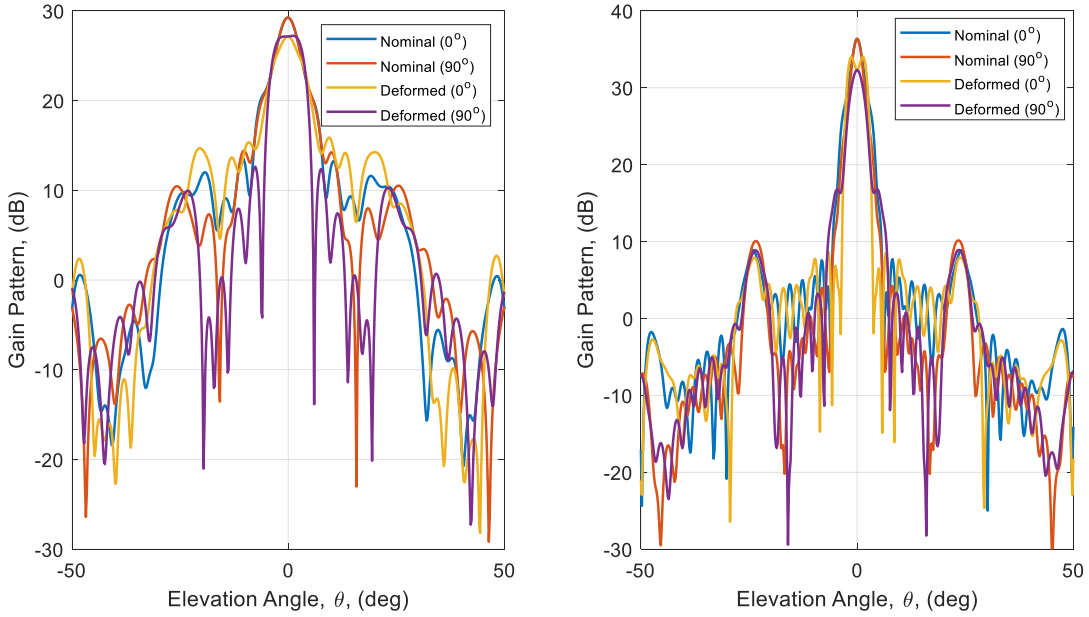

Figure 4.12: Systematic Radiation Patterns (n = 2) with RMS = λ/10 for 20λ (Left) and 40λ (Right) Reflectors

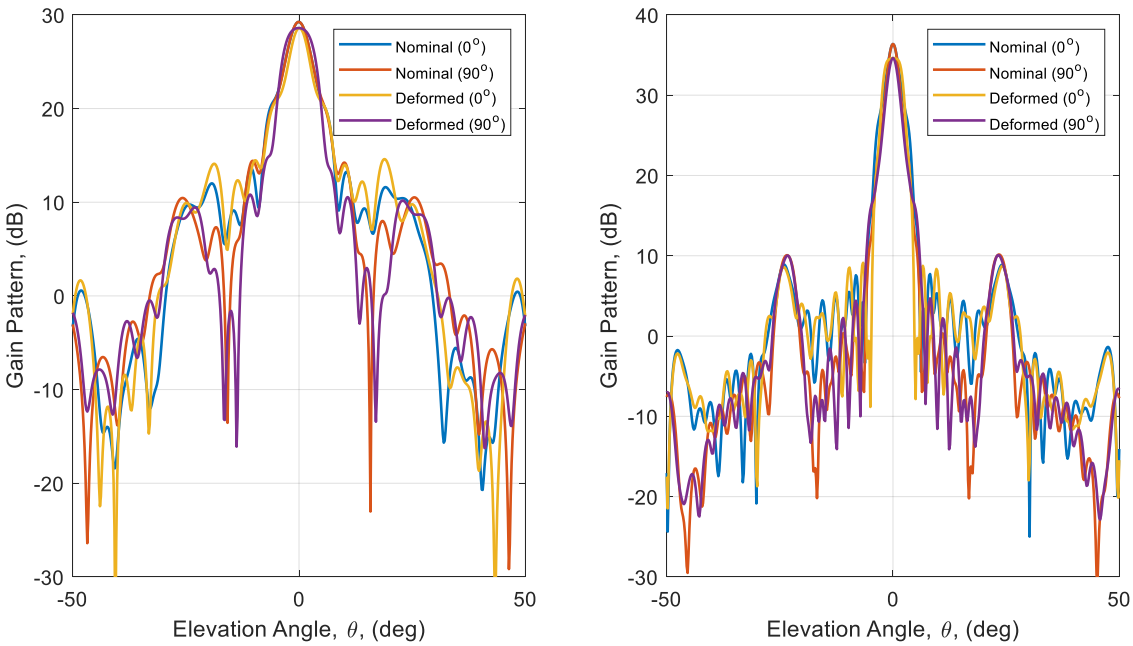

Figure 4.13: Systematic Radiation Patterns (n = 2) with RMS = λ/20 for 20λ (Left) and 40λ (Right) Reflectors

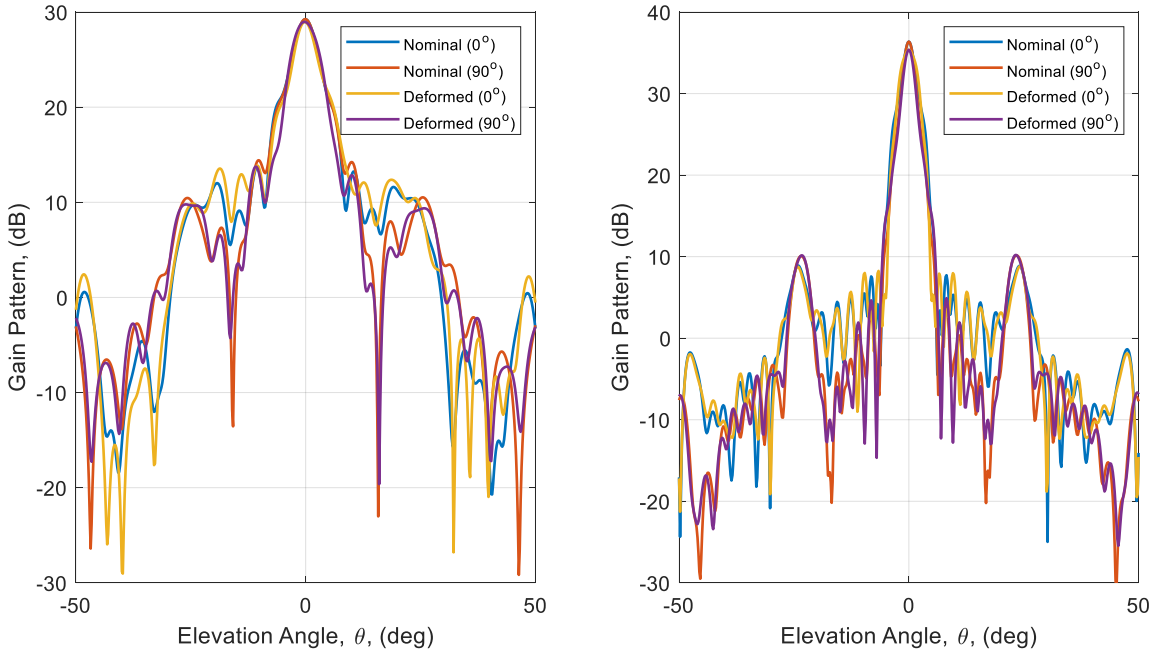

Figure 4.14: Systematic Radiation Patterns (n = 2) with RMS = λ/30 for 20λ (Left) and 40λ (Right) Reflectors

Table 4.5: Average Values for the Reflector Antenna Performance Properties for 20λ and 40λ Surfaces Subjected to Systematic Errors (n = 2)

	Max Gain (dB)		Relative SLL (dB)		HPBW (deg.)	
RMS	**20λ**	**40λ**	**20λ**	**40λ**	**20λ**	**40λ**
λ/10	27.1	34.0	-13.4	-19.6	7.4	4.6
λ/15	27.8	34.4	-14.3	-26.6	7.2	4.5
λ/20	28.6	34.6	-14.7	-26.3	7.0	4.3
λ/30	29.0	35.4	-15.4	-26.2	5.8	3.8
λ/40	29.3	35.7	-15.0	-26.2	5.4	3.4
λ/50	29.3	35.9	-14.9	-26.2	5.4	3.2
λ/60	29.4	36.0	-15.5	-26.2	5.2	3.0
λ/70	29.4	36.0	-15.4	-26.2	5.3	2.9
Nominal	29.3	36.4	-15.5	-27.5	4.9	2.5

For systematic errors utilizing two node lines, the observed trends and losses follow the results of the three-node line reflector with an exception in the SLL of the higher error cases (λ/10 to λ/40). This observation is seen where the three node line results show a much higher increase

in side lobe for these higher surface error cases. As well, the two node line cases are shown to have higher HPBW (~ 1^{o}) values most likely due to distribution of the errors being more condensed and symmetrical as shown in Figure 3.4.

When comparing the systematic error results to the random error results, the larger reflector exhibits performance fairly similar to the random smooth error case. On the other hand, the smaller reflector with systematic errors converged much closer to the nominal gain and HPBW than either of the random distortion cases.

To better visual and compare the trends in performance for each of the cases, the following sections provides plots of the data contained in Tables 4.2-4.5.

4.2.4 Comparison of the Various Deformation Trends Modeled

Figure 4.15 through Figure 4.17 present plots for each of the pattern metrics summarized in Table 4.2 through Table 4.5. Figure 4.15 presents the maximum gain for both the 20λ and 40λ reflectors, Figure 4.16 presents the relative SLL, and Figure 4.17 presents the HPBW.

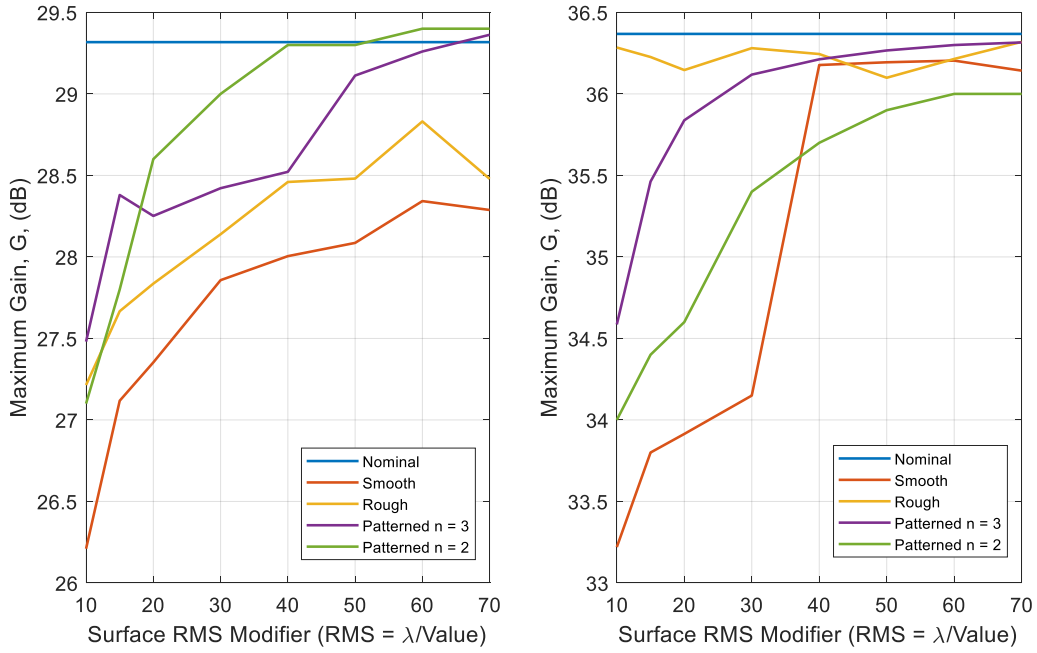

Figure 4.15: Maximum Gain Trends of 20λ (Left) and 40λ (Right) Reflectors Subject to Random and Systematic Errors

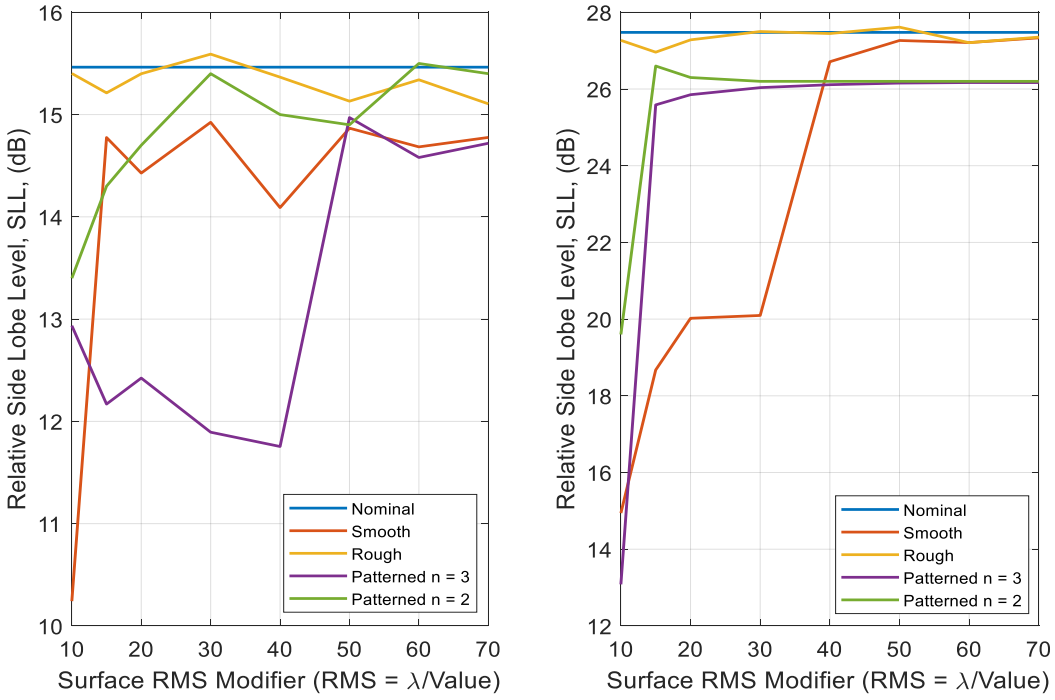

Figure 4.16: Relative Side Lobe Level Trends of 20λ (Left) and 40λ (Right) Reflectors Subject to Random and Systematic Errors

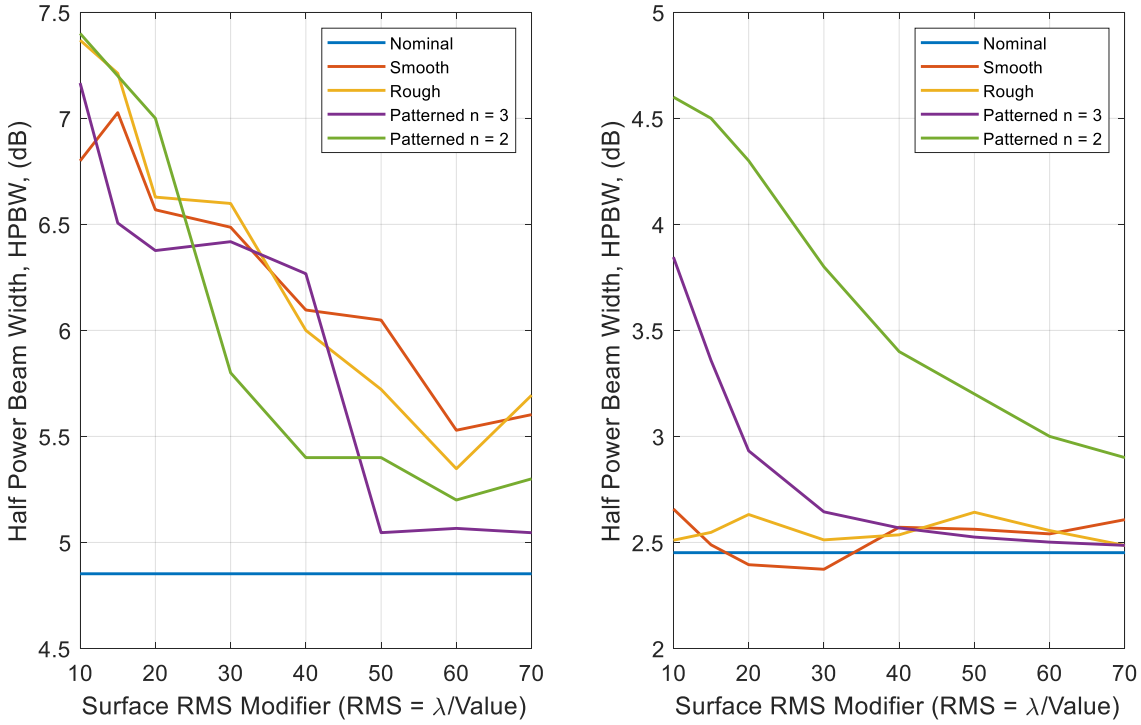

Figure 4.17: Half Power Beam Width Trends of 20λ (Left) and 40λ (Right) Reflectors Subject to Random and Systematic Errors

From the trends displayed in Figures 4.15-4.17, a qualitative observation of the gain loss shows that the larger reflector (40λ) converges to the nominal reflector values at a quicker rate than that of the smaller reflector (20λ). In the case of the 20λ reflector, each of the gain trends show similar trajectory towards the nominal values with the smooth surface error case maintaining ~0.5 dB greater loss in gain compared to the rough errors. Similarly, the gain loss from the rough errors is ~0.5 dB greater when compared to the systematic errors. In contrast, the 40λ reflector results have variable trends depending on the error case. As shown in Figure 4.12, the rough surface error case is shown to result in a relatively constant 0.2 dB gain loss across all RMS values. Smooth surface errors are shown to have a drastically larger loss for RMS greater than λ/40, and the gain loss at λ/10 is comparable for both the 20λ and 40λ reflectors (~3 dB); however, unlike the 20λ reflector, the 40λ reflector gain converges to within 0.2 dB of the nominal value by λ/40.

The n=3 systematic error show in a steady logarithmic trend starting at a gain loss 1.8 dB and converging to a gain loss of 0.1 dB, while the n=2 surface has a slightly lower convergence of 0.4 dB.

In the case of SLL, both reflectors are relatively insensitive to rough surface errors. The rough surface error cases are shown to be within ~0.19 dB and ~0.15 dB of the nominal values for the 20λ and 40λ reflectors for all RMS values, respectively. By contrast, both the smooth and systematic error cases exhibit large degradations at a surface RMS of λ/10 as the main beam tends to vary in shape due to the large surface variation. Interestingly, only the smooth error case for the 40λ reflector converges to within 0.5 dB of the nominal values for even the smallest errors. This would imply that even the smallest of surface errors in these cases results in an increase in SLL.

The half power beam width degradation due to surface errors has a similar trend for the smooth and rough surface errors for both the 20λ and 40λ reflectors; however, the natures of these trends are different. This is shown through the linear decrease of the HPBW in the small reflector from ~7^{o} to ~5.6^{o}, whereas the large reflector maintains a relatively constant 0.1^{o} increase in HPBW for both the smooth and rough surface error cases. The n=3 systematic errors follow the same trends exhibited in the random cases on the 20λ reflector until about λ/40 where the HPBW starts to narrow at a faster rate than for the random errors. The opposite is true for the larger reflector. The systematic HPBW is over a full degree larger at λ/10, but then converges to within 0.05^{o} of the random cases at λ/40. For the n = 2 small reflector, the trend generally follows the other designs, while there is a very noticeable increase in HPBW for the 40λ. This increase in HPBW for the n = 2 systematic errors are shown to range from 0.5^{o} at λ/70 to 1^{o} at λ/30 compared to the values seen in the n = 3 case.

From the plots, it is clear that the large reflector is relatively insensitive to rough surface errors. This is significant for two reasons. The first reason is that this indicates that the larger the reflector, the lower the pattern sensitivity is to surface errors, especially with lower correlation length (i.e. “rough surface error”). The larger reflector was also generally less sensitive to small surface errors than the smaller reflector. This is illustrated by the fact that the 20λ reflector maintained ~1 dB in gain loss, ~0.5 dB increase in SLL, and 0.5^{o} increase in HPBW for surface errors with RMS values as small as λ/70.

The second significant point illustrated by the large reflector’s insensitivity to RMS is that clearly the metric of RMS alone is not sufficient to characterize expected changes in the radiation pattern. This is made obvious not only due to the fact that the rough RMS generally resulted in the best performance, but also by the fact that the systematic error often followed a different trend than the random errors. The difference in gain and HPBW for the case of the systematic errors also illustrates this same point. Furthermore, the increase seen in the HPBW of the systematic errors stems from how these errors are distributed and the maximum deformation of the surfaces in the n = 2 surfaces compared to the n = 3 surfaces. This distribution of errors is shown in Figure 3.5. The results in this chapter suggest that predictions could be off by as much as 1 dB for gain loss, 1.5 dB for SLL, and 0.5^{o} for RMS values as small as λ/70 if the nature of the surface error is not also considered.

5 Theoretical Comparison

As discussed previously, the antenna tolerance theory developed by Ruze is a common and straightforward approach for predicting reflector antenna performance in the presence of surface errors. The radiation patterns using Ruze's theory were determined for both the 20λ and 40λ reflector antennas using Equation 2.7. The resulting patterns are shown in Figure 5.1 and Figure 5.2. Because Equation 2.7 is a function of the surface RMS, Ruze's approach to determining the resultant radiation pattern is deterministic, and thus only one instance needs to be calculated.

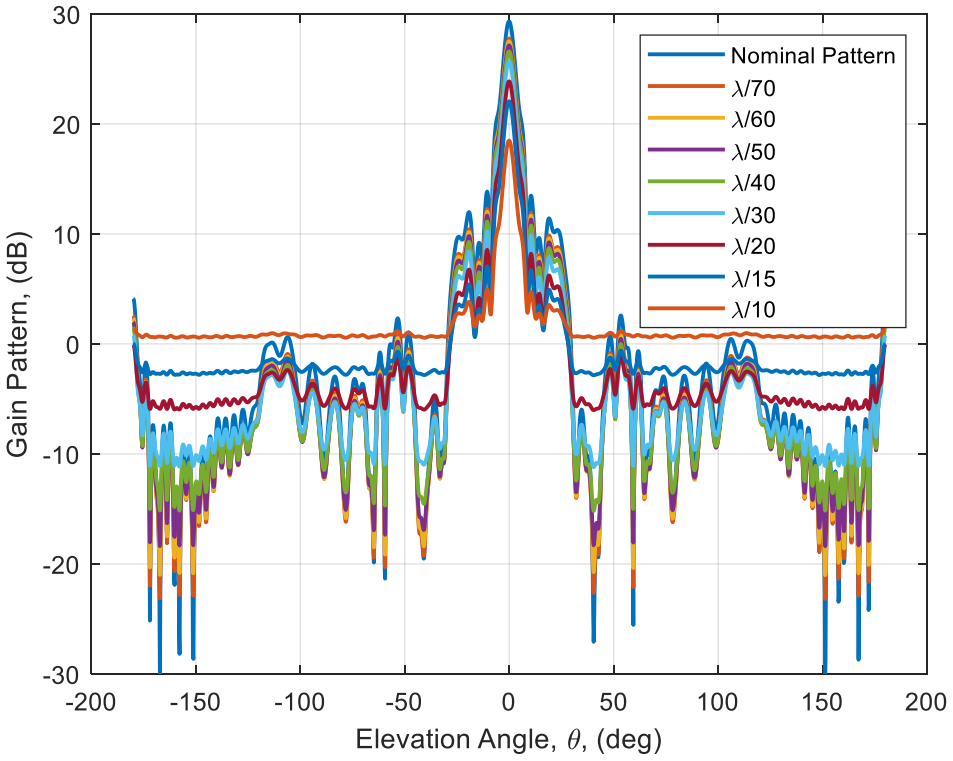

Figure 5.1: 20λ Reflector Antenna Radiation Patterns with Varying RMS Produced Utilizing the Antenna Tolerance Theory

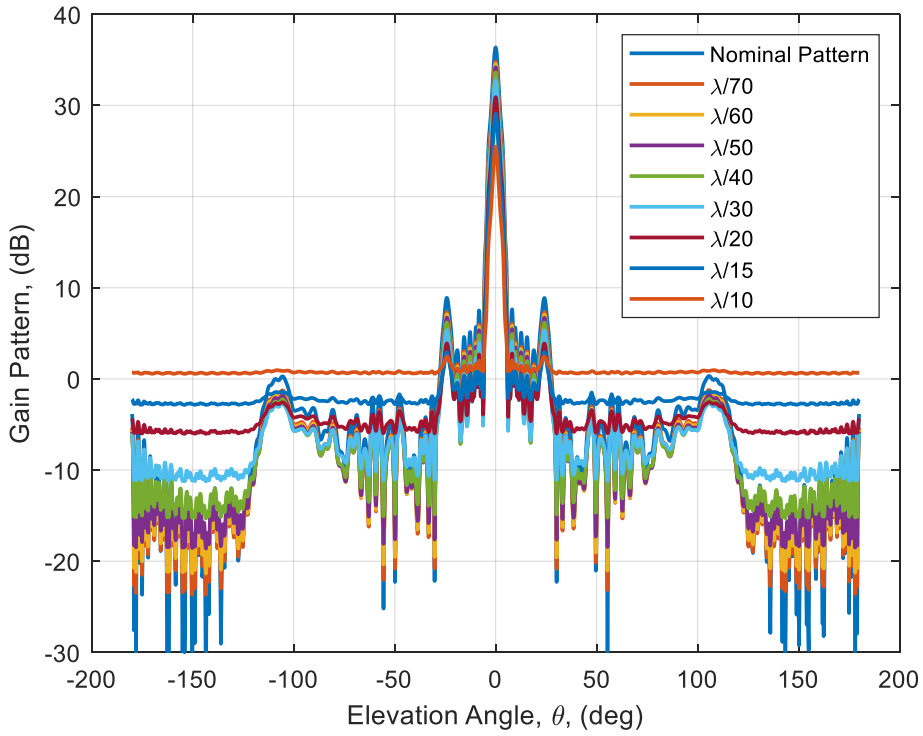

Figure 5.2: 40λ Reflector Antenna Radiation Patterns with Varying RMS Produced Utilizing the Antenna Tolerance Theory

From the radiation patterns constructed utilizing the Ruze method, the resulting trends of maximum gain and relative SLLs are displayed in Figure 5.3 and Figure 5.4 for comparison to the random and systematic error results shown in Section 4. The resulting beam width trends are not displayed as the Ruze method results show negligible variation in the HPBW for all surface RMS cases. Table 5.1 summarizes all the error cases results while showing the specified trend in beam width.

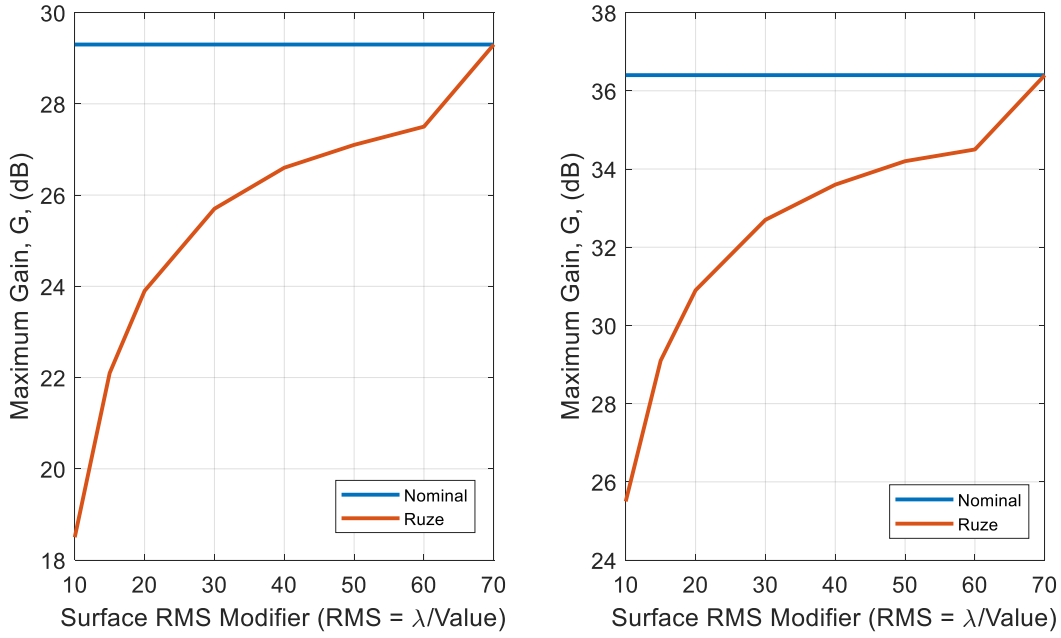

Figure 5.3: Maximum Gain Trend of 20λ (Left) and 40λ (Right) Reflectors Utilizing Ruze's Method

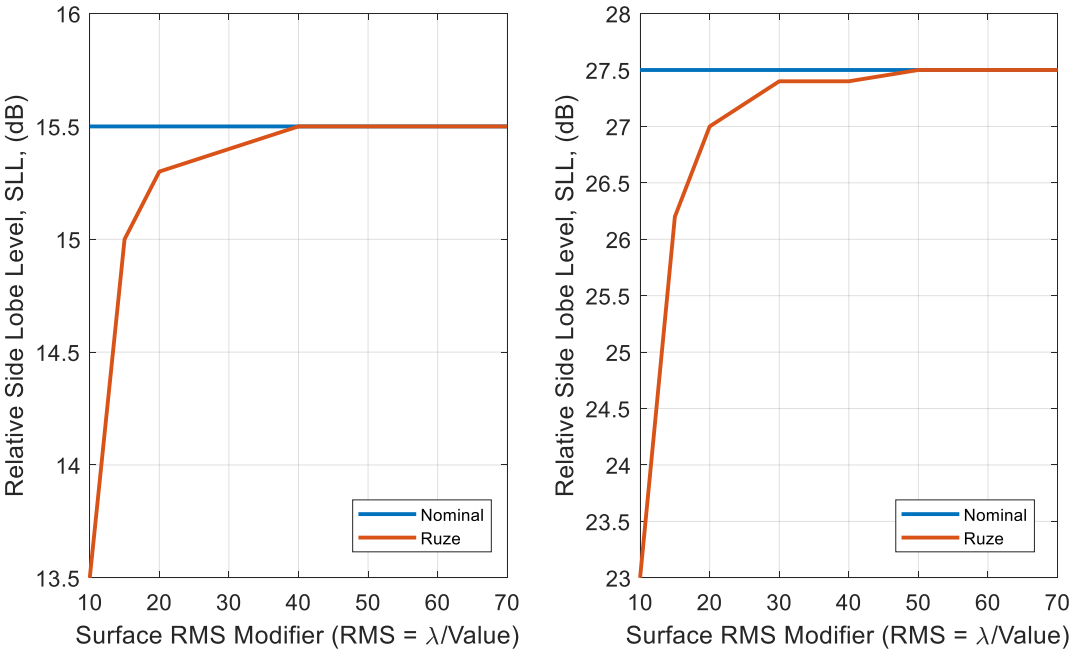

Figure 5.4: Relative SLL Trend of 20λ (Left) and 40λ (Right) Reflectors Utilizing Ruze's Method

Table 5.1: Average Values for the Reflector Antenna Performance Properties for 20λ and 40λ Surfaces with Given RMS utilizing Ruze's Technique

	Max Gain (dB)		Relative SLL (dB)		HPBW (deg.)	
RMS	**20λ**	**40λ**	**20λ**	**40λ**	**20λ**	**40λ**
λ/10	18.5	25.5	-13.5	-23	4.9	2.5
λ/15	22.1	29.1	-15	-26.2	4.9	2.5
λ/20	23.9	30.9	-15.3	-27	4.9	2.5
λ/30	25.7	32.7	-15.4	-27.4	4.9	2.5
λ/40	26.6	33.6	-15.5	-27.4	4.9	2.5
λ/50	27.1	34.2	-15.5	-27.5	4.9	2.5
λ/60	27.5	34.5	-15.5	-27.5	4.9	2.5
λ/70	29.3	36.4	-15.5	-27.5	4.9	2.5
Nominal	29.3	36.4	-15.5	-27.5	4.9	2.5

In comparing the results presented in Section 4 to the Ruze method results summarized in Figures 5.3 and 5.4 and Table 5.1, the Ruze technique appears to produce results that more closely follow the observed trends of the smooth and systematic surface error cases. This observation is most clearly seen by the logarithmic gain curve shown in both Figure 5.3 and Figure 4.12. This trend, however, does not continue from a surface RMS of λ/60 to λ/70, where a jump to the nominal value is observed. Similarly, SLLs shown in Figure 5.4 resemble the results of smooth and systematic errors presented in Figure 4.13 where a large leap in SLL is experienced above an RMS of λ/20, then settling near the nominal value.

For the simulated smooth RMS surfaces, gain drops of 3.1 dB and 3.2 dB were observed for the 20λ and 40λ antennas, respectively, when RMS was equal to λ/10; however, the Ruze calculations show an almost 11 dB loss. This difference in gain loss prediction is also observed for RMS values as small as λ/60. The random error cases in Figure 4.12 indicate a gain loss of ~1 dB for the 20λ reflector, while the Ruze method is shown to produce a 2 dB loss. This overprediction in gain loss is a well-known limitation of antenna tolerance theory [9][10][12], and in this instance,

it is observed across all RMS up until $\lambda/70$ when the values converge to nominal values. For SLL, the Ruze method largely under predicts the increase in SLL when compared to the smooth errors case but over predicts as compared to the rough error case. This underprediction in the smooth error SLLs is most well seen in the severity of the performance loss at λ/10, where Ruze predicts an increase of 2 dB and 4.5 dB for the 20λ and 40 reflectors, respectively. The FEA results for the same case show a loss of 5.3 dB and 12.6 dB, respectively. Furthermore, Ruze's method shows the SLLs recover much quicker than the smooth and systematic surface error cases. This is shown in the Ruze results reaching the nominal value at λ/40, where the SLL in random error surfaces are only shown to recover to the nominal value in the rough cases.

When comparing the results in Section 5 to those in Section 4, it is clear that Ruze's method over predicts gain loss in all cases, with the exception of the λ/70 case. SLL level predictions are similar to the random rough surface errors; however, this is due to the fact that the FEA results showed very little sensitivity to surface errors. Finally, it is clear that Ruze's method has no ability to predict changes in the HPBW. Although Zarghamee in [8] did show the prediction in HPBW may be achieved from modifying the error distribution in the Ruze's method to more accurately predict the illumination function.

6 Conclusions and Recommendations

Through the results presented in Section 4 and the theoretical comparison presented in Section 5, the following conclusions are made about the sensitivity of reflector antennas to the various surface errors as well as the limitations of Ruze's antenna tolerance theory.

- The results show that through FEA analysis, the 20λ and 40λ reflectors are much more sensitive to the smooth surface errors (variations in the surface with higher correlation lengths) than rough surface errors (lower correlation lengths).
- As well, the results show the larger the reflector surface, the lower the performance sensitivity is to surface errors. This is illustrated by the FEA results having a faster recovery to the nominal performance values for the larger reflector.
- The metric of RMS alone is not sufficient to characterize expected changes in the radiation pattern. Classification of the surfaces utilizing correlation lengths would show the distribution of the errors on the surface. With this, the results show that for the various surface error types, categorized with correlation lengths, the predicted values could be off by as much as 1 dB for gain loss, 1.5 dB for SLL, and 0.5^{o} for RMS values as small as λ/70. As well, Ruze's method over predicts gain loss, under predicts SLL increases for surface errors with large correlation length, and is incapable of capturing any changes to half-power beam width.

6.1 Recommendations

The following are recommendations for follow-up studies based on the results of this work:

- Further exploration of other commonly utilized reflector analysis techniques such as the aperture distribution and current distribution methods. These methods are

more comprehensive than Ruze's antenna tolerance theory. This would provide a better comparison to more commonly used techniques and provide a more insightful comparison of the FEA method utilized in this paper.

- Increase in the number of random error cases to capture smaller deformation steps as to more accurately establish the trends shown in Section 4. Several large jumps were observed between RMS cases, and the smaller step size will help refine the trends.
- Assess a larger range of reflectors size to verify the trends of increasing reflector surface sizes on performance metrics.
- Further establish the trends seen with differing surface types by simulating additional surfaces with differing errors correlation lengths. This will better resolve the trends seen in the results of the smooth error cases.
- The default convergence criteria in in HFSS Ver. 19 is the maximum change in the magnitudes of the S-parameters between each adaptive mesh operation. Though the S-parameter is the recommended convergence approach for most simulations, it tends to converge faster than the field quantities (gain, side lob levels, or HPBW). It is recommended to re-simulate a subset of the designs to verify convergence for the field quantifies. One approach to do this is using the Expression Cache in HFSS. Using this approach field quantities can be directly used as the convergence criteria. Though alternate convergence criteria may be specified-ANSYS HFSS recommends the use of the default S-Parameter convergence criteria and simply increasing the number of required converged passes as another means for ensuring field convergence [32].

References

[1] Warren P., Steinbeck J., and Minelli R., “Large, Deployable S-Band Antenna for a 6U Cubesat,” AIAA Conference on Small Satellites, 2015.

[2] Arya, M., Sauder, J. F., Hodges, R., and Pellegrino, S., “Large-Area Deployable Reflectarray Antenna for CubeSats,” AIAA SciTech Forum, Jan. 2019.

[3] Chahat, N., Hodges, R. E., Sauder, J., Thomson, M., and Rahmat-Samii, Y., "The Deep-Space Network Telecommunication CubeSat Antenna: Using the deployable Ka-band mesh reflector antenna," IEEE Antennas and Propagation Magazine, Vol. 59, April 2017, pp. 31-38.

[4] Mendoza Strilchuk, P., “Structural-Electromagnetic Simulation Coupling and Conformal Antenna Design Tool,” M.S. Dissertation, Dept. of Aerospace Engineering, Univ. of Kansas, Lawrence, KS, May 2018.

[5] Ruze J., "Antenna tolerance theory—A review," in *Proceedings of the IEEE*, Vol. 54, April 1966, pp. 633-640.

[6] *ANSYS Electronics Desktop HFSS*, Software Package, Ver. 19.1, 2019. Available from https://www.ansys.com/products/electronics/ansys-hfss.

[7] Boonsalee, S., “Effects of random surface errors on the performance of paraboloidal reflectors,” Dept. of Electrical Engineering, Massachusetts Institute of Technology, July 2001.

[8] Balanis, C., Antanna Theory, 4th ed., John Wiley & Sons, Inc., Hoboken, New Jersey, 2016.

[9] Zarghamee M., "On antenna tolerance theory," IEEE Transactions on Antennas and Propagation, Vol. 15, Nov. 1967, pp. 777-781.

[10] Cheng D., "Effect of arbitrary phase errors on the gain and beamwidth characteristics of radiation pattern," IRE Transactions on Antennas and Propagation, Vol. 3, July 1955, pp. 145-147.

[11] Rahmat-Samii Y., "An efficient computational method for characterizing the effects of random surface errors on the average power pattern of reflectors," in IEEE Transactions on Antennas and Propagation, Vol. 31, Jan. 1983, pp. 92-98.

[12] Hao Ling, Yuen Lo and Rahmat-Samii Y., "Reflector sidelobe degradation due to random surface errors," in IEEE Transactions on Antennas and Propagation, vol. 34, Feb. 1986, pp. 164-172.

[13] Jervase J., and Ghobrial S., "Axial cross polarization in reflector antennas with surface errors of large correlation diameter," in IEEE Transactions on Antennas and Propagation, Vol. 31, July 1983, pp. 662-665.

[14] Ghobrial S., "Axial cross polarization in reflector antennas with surface imperfections," IEEE Transactions on Antennas and Propagation, Vol. 28, Sept. 1980, pp. 610-616.

[15] Tripp V., "A new approach to the analysis of random errors in aperture antennas," IEEE Transactions on Antennas and Propagation, Vol. 32, Aug. 1984, pp. 857-863.

[16] Gao, S., Rahmat-Samii, Y., Hodges, R. E., and Yang, X., “Advanced antennas for small satellites,” Proc. IEEE, Vol. 106, Mar. 2018, pp. 391–403.

[17] Sauder J. F. el al, “Deployment Mechanisms for High Packing Efficiency One Meter Reflectarray Antenna (OMERA)," AIAA Scitech Forum, Jan. 2019.

[18] Hodges E. R.et al, “The ISARA Mission – Flight Demonstration of a High Gain Ka-Band Antennafor 100Mbps Telecom,” AIAA Conference on Small Satellites, 2018.

[19] Hodges R. E., Chahat N. E., Hoppe D. J., and Vacchione J. D., "The Mars Cube One deployable high gain antenna," 2016 IEEE International Symposium on Antennas and Propagation (APSURSI), Fajardo, 2016, pp. 1533-1534.

[20] Cutler C. C., "Parabolic-Antenna Design for Microwaves," Proceedings of the IRE, vol. 35, Nov. 1947, pp. 1284-1294.

[21] Silver, S., Microwave Antenna Theory and Design (MIT Radiaion Lab. Series, Vol. 12), McGraw-Hill, New York, 1949.

[22] Wu, S. and Rahmat-Samii, Y., "Beam efficiency of large reflector antennas subject to correlated random surface errors," International Symposium on Antennas and Propagation Society, Merging Technologies for the 90's, Dallas, TX, USA, Vol. 1, pp. 144-147, 1990.

[23] Stutzman, W. L., and Thiele, G. A., Antenna Theory and Design: Second Edition. John Wiley & Sons, New York, 1998.

[24] Safak, M., "Limitations on reflector antenna gain by random surface errors, pointing errors, and the angle-of-arrival jitter," in IEEE Transactions on Antennas and Propagation, vol. 38, Jan. 1990, pp. 117-121.

[25] Skolnik, T M. I., Large Antenna Systems. In R. E. Collin and F. J. Zucker, editors, Antenna Theory: Part 2, pages 655-674. McGraw-Hill, New York, 1969.

[26] *MathWorks MATLAB*, Software Package, Ver. R2020a, 2020. Available from https://www.mathworks.com/products/matlab.html/.

[27] Ogilvy, J. A. and Foster, J. R., “Rough surfaces: gaussian or exponential statistics?,” Phys. D: Appl. Phys. 22, 1989, pp. 1243-1251.

[28] *Siemens NX MATLAB*, Software Package, Ver. 1872, 2019. Available from https://www.plm.automation.siemens.com/global/en/products/nx/

[29] Xu, S., Rahmat-Samii, Y., and Imbriale, W. A., "Subreflectarrays for Reflector Surface Distortion Compensation," IEEE Transactions on Antennas and Propagation, Vol. 57, Feb. 2009, pp. 364-372.

[30] Bahadori, K. and Rahmat-Samii, Y., "Characterization of effects of periodic and aperiodic surface distortions on membrane reflector antennas," *IEEE Transactions on Antennas and Propagation*, Vol. 53, Sept. 2005, pp. 2782-2791

[31] Silvestro, J., "Hybrid Finite Element Boundary Integral Method," White Paper, 2010, ANSYS, Inc., Canonsburg, PA, USA.

[32] *ANSYS Electronics Desktop HFSS*, "ANSYS HFSS for Antenna Simulation," White Paper, 2014, ANSYS, Inc., Canonsburg, PA, USA.

Appendix A

To show the Variation in the RMS for each of surface types using the NX deviation gage tool, Table A.1 provides the maximum change in the RMS for each surface variant. Through NX, about 50 points where taken from each 20λ reflector surface. With this data, the RMS, and subsequently percent change in RMS, were calculated and provided in the table.

Table A.1: Maximum Variation in Surface RMS

	Maximum Variance in RMS	
RMS	**Rough**	**Smooth**
λ/10	1.282%	1.556%
λ/15	1.978%	1.859%
λ/20	1.620%	1.821%
λ/30	1.985%	1.069%
λ/40	1.345%	1.067%
λ/50	1.422%	1.261%
λ/60	1.828%	1.959%
λ/70	1.629%	1.539%

Appendix B

To verify, that the change in simulation approach between the 20λ and 40λ reflector did not influence the results, the 20λ reflector was simulated using both approaches and the results are compared here. Tables B.1 and B.2 summarize the results from the FEA analysis of the 20λ reflector utilizing a FEBI region solution and a Hybrid IE Region, respectively. These results from the differing model setups show the differing setups have less than 0.1 dB change in maximum gain, 0.1 dB change in SLL, and 0.1^{o} change in beamwidth. The results verify the errors that may arise due to modeling technique utilized for the 20λ reflector (FEBI Region) and the 40λ (Hybrid IE) are negligible for this study. Lastly, Figure A.1 shows the radiation patterns for each of the reflectors modeled utilizing the differing modeling techniques.

Table B.1: Comparison Between HFSS Symulation Methods for Random Smooth Surface Errors

	Max Gain (dB)		Relative SLL (dB)		HPBW (deg.)	
RMS	**FEBI Region**	**Hybrid IE**	**FEBI Region**	**Hybrid IE**	**FEBI Region**	**Hybrid IE**
λ/10	26.2	26.3	-10.2	-10.2	6.8	6.9
λ/15	27.1	27.2	-14.8	-14.8	7.0	7.1
λ/20	27.4	27.5	-14.4	-14.5	6.6	6.6
λ/30	27.9	28.0	-14.9	-14.9	6.5	6.6
λ/40	28.0	28.0	-14.1	-14.2	6.1	6.2
λ/50	28.1	28.2	-14.9	-14.9	6.0	6.0
λ/60	28.3	28.3	-14.7	-14.7	5.5	5.6
λ/70	28.3	28.4	-14.8	-14.9	5.6	5.7
Nominal	29.3	-	-15.5	-	4.9	-

Table B.2: Comparison Between HFSS Symulation Methods for Random Rough Surface Errors

	Max Gain (dB)		Relative SLL (dB)		HPBW (deg.)	
RMS	**FEBI Region**	**Hybrid IE**	**FEBI Region**	**Hybrid IE**	**FEBI Region**	**Hybrid IE**
λ/10	27.2	27.3	-15.4	-15.5	7.4	7.5
λ/15	27.7	27.7	-15.2	-15.3	7.2	7.2
λ/20	27.8	27.9	-15.4	-15.4	6.6	6.7
λ/30	28.1	28.1	-15.6	-15.7	6.6	6.7
λ/40	28.5	28.6	-15.4	-15.4	6.0	6.0
λ/50	28.5	28.6	-15.1	-15.2	5.7	5.7
λ/60	28.8	28.8	-15.3	-15.4	5.3	5.4
λ/70	28.5	28.6	-15.1	-15.1	5.7	5.7
Nominal	29.3	-	-15.5	-	4.9	-

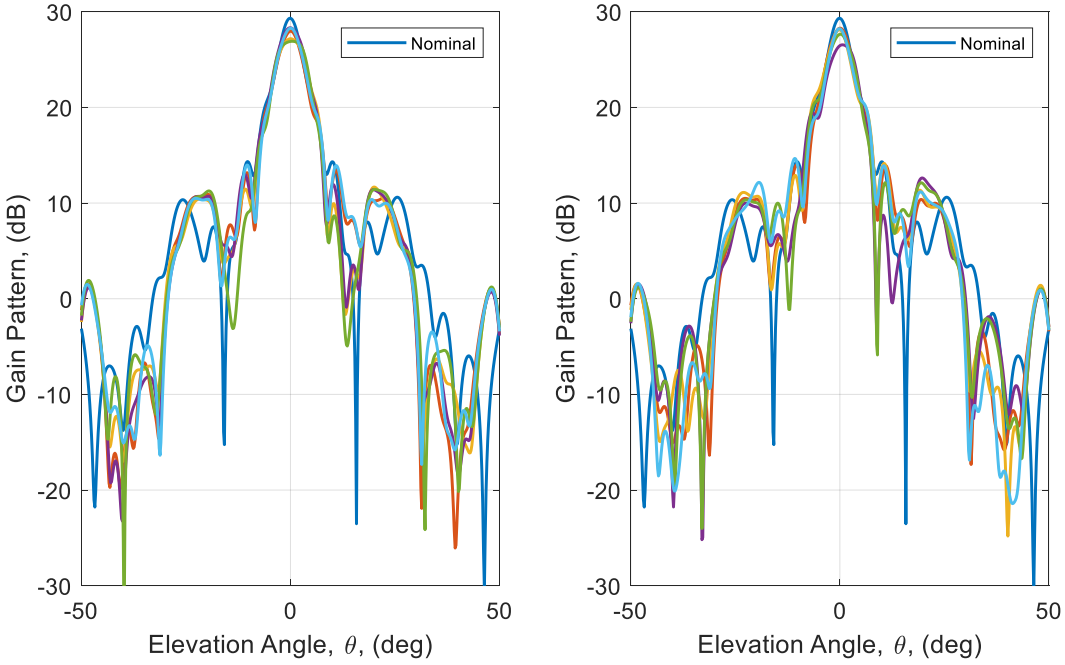

Figure B.1: 20 Reflector FEBI Region Modeling (Left) Compared to the Hybrid IE Modeling (Right)